IVYSPRING INTERNATIONAL PUBLISHER

Theranostics

2026; 16(3): 1295-1327. doi: 10.7150/thno.121977

Review

Design of prodrugs with reactive oxygen species as activators and their application in tumor therapy

Jiaqi Xing[1,#], Wenjuan Lu[1,#], Yubing Zhang[1], Chen Yang[1], Jikai Yang[1], Jing Shi[2,✉], Yanfeng Wang[1,✉]

1. State Key Laboratory of Advanced Drug Delivery and Release Systems, Key Laboratory for Biotechnology Drugs of National Health Commission, Key Laboratory of Rare and Rare Diseases in Shandong Province, School of Pharmacy (Institute of Pharmacy) of Shandong First Medical University, Jinan, Shandong 250117, China.
2. Department of Pharmacy (Shandong Key Traditional Chinese Medical Discipline of Clinical Chinese Pharmacy), Shandong Cancer Hospital and Institute, Shandong First Medical University and Shandong Academy of Medical Sciences, Jinan 250117, China.

[#] These authors contributed equally to this work.

✉ Corresponding author: Y. F. Wang and Jing Shi, Email: wangyanfeng@sdfmu.edu.cn.

Received: 2025.07.18; Accepted: 2025.10.10; Published: 2026.01.01

Abstract

Major challenges lie in the precise management (encompassing diagnosis and treatment) of malignant neoplasms. Traditional chemotherapy faces restrictions in clinical use because of its ineffective targeting and significant toxicity, along with side effects. Notably, the ROS levels are observably elevated in cancer cells compared to healthy tissues, which presents a distinct opportunity for the creation of prodrugs that respond to ROS. This article systematically reviewed the research progress on ROS-responsive small molecule prodrugs and nanodelivery systems (including polymer/inorganic nanoparticles and hydrogels) over the past five years and elaborated in detail on the design principles based on seven key activation mechanisms. By combining ROS responsiveness with TME specificity, these systems have achieved precise controlled drug release, significantly reduced toxic and side effects, and demonstrated multiple synergistic effects of chemotherapy, immunotherapy, and photodynamic therapy. Additionally, some systems integrate theranostic and imaging functions, allowing real-time observation of the drug release. Subsequently, the latest progress in the field from molecular design to preclinical research was summarized, and the promise of ROS-responsive systems for clinical applications was emphasized. It directs the creation of prodrugs that are highly specific and supports the advancement of multi-responsive theranostic platforms, thereby paving the way for improved precision in the diagnosis and treatment of tumors.

Keywords: ROS, prodrugs, nanoparticles, tumor treatment

1. Introduction

A crucial obstacle in global public health is the growing importance of early detection and management of malignant tumors [1]. By the year 2025, it is forecasted that there will be 2 million newly diagnosed cases of cancer, with cancer-related deaths reaching 600,000. In 2022, the survival rate increased by 34% compared to 1991, but it still adds up to a huge burden. Currently, traditional methods for treating cancer mainly consist of surgery, chemotherapy, radiotherapy, and immunotherapy; however, each of these treatments has notable limitations [2,3]. Due to the lack of accurate identification of tumor boundaries, surgical resection often faces a dilemma [4]: incomplete resection or excessive resection. The former may lead to tumor metastasis or recurrence, while the latter tends to impair the normal physiological function of tissues and organs. Although systemic chemotherapy and radiotherapy have broad-spectrum antitumor effects, their mechanisms of cytotoxicity, which are not selective, may lead to harm to healthy tissues and organs [5]. Immunotherapy offers specific targeting and minimal toxic side effects, but the high cost makes it challenging to popularize on a large scale [6]. It is worth noting that in 2024, there were 2,162 oncology trials globally, coming in at 41% of all clinical trials. Moreover, solid tumors remain a key focus of research and development, reflecting the pressing demand within tumor therapy. Stimuli-responsive prodrugs and drug delivery systems (DDS) open new paths for

tumor treatment. By precisely regulating drug activity and targeted delivery, these systems significantly enhance therapeutic efficacy and reduce systemic toxicity [7,8]. Its activation methods are rich and diverse, such as the widely applied exogenous stimulus regulation strategy. The Perylene Diimide-Based Photoacid Generator (PBI-PAG) can respond to green light/red light (560-605 nm), efficiently release acid and photosensitizers, and achieve deep tissue penetration by utilizing the long wavelength. The synergistic effect of the released acid and photosensitizers enhance the antitumor effect [9]. Camptothecin prodrug NO-CPT can be activated by the hydrated electrons generated by radiotherapy, achieving the synergistic effect of radiotherapy and chemotherapy [10]. The palladium-nanomodified microneedle patch delivers prodrugs to the tumor location through biorthogonal reactions catalyzed by transition metals, featuring high targeting efficiency and minimal damage to normal tissues [11]. The specificity of the tumor microenvironment (TME) as a natural trigger signal is also widely applied [12], which can reduce off-target activation by leveraging the difference between the TME and normal tissues, including reactive oxygen species (ROS), reactive nitrogen species (RNS), levels of thiols, viscosity, pH, and polarity [13]. Previous reports have shown that cabazitaxel (CTX) and chitosan (CS) are conjugated through a glutathione (GSH)-sensitive disulfide maleimide (DTM) for treating breast cancer [14]. In addition, acid-responsive hydrazone bonds are employed to prepare targeted nanomedicines, PEG-Dendron-EPI@TPP-LND, which exerted a synergistic effect by inhibiting oxidative phosphorylation (OXPHOS) and enhancing the chemotherapy efficacy of the epirubicin (EPI) prodrug, leading to enhanced treatment outcomes for triple-negative breast cancer [15].

ROS are essential in biochemical reactions and sustaining redox homeostasis inside the cell [16]. Appropriate ROS levels are crucial for maintaining immune responses, regulating cellular signaling, and ensuring cellular homeostasis [17,18]. In various diseases, there is often an abnormal increase in ROS levels [19], which is not only an essential indicator of the pathological characteristics of diseases but also provides key targets for elucidating disease mechanisms and formulating treatment strategies [20,21]. Disease treatment targeting ROS has become a research hotspot. For instance, using the pathologically elevated ROS levels at the infection site as a "biological switch", a supramolecular self-assembly system regulated by ROS has been constructed to achieve the inhibition of bacterial infection [22]. The combination of ROS-induced supramolecular assembly with biorthogonal reactions enables the spatiotemporally controlled release of the inhibitory neurotransmitter GABA, thereby inhibiting epileptic seizures [23]. Elevated ROS levels can also serve as a potential target for enhancing the precision of tumor diagnosis and treatment [24]. The reasons for the increase in ROS levels in tumors can be divided into the following aspects: 1. Abnormal metabolism: The energy requirements rise due to heightened metabolic activity in tumor cells, which promotes mitochondrial production capacity, breaks the balance of adenosine triphosphate (ATP) metabolism in the cell, and leads to a decrease in the efficiency of oxidative phosphorylation (a key process for efficient ATP production) [18,25,26]. Electron transfer in the electron transfer chain (ETC) is blocked, and it is easier to react with oxygen to generate ROS, which directly leads to an increase in intracellular ROS levels [27]. 2. TME factors: The TME is often in a state of hypoxia [28,29]. This triggers the activation of hypoxia-inducible factor-1 (HIF-1), which enhances the production of ROS. At the same time, the new ROS will upregulate the expression of HIF-1, establishing a positive feedback mechanism [30]. Furthermore, immune cells, including macrophages and T lymphocytes, that gather around tumor cells secrete inflammatory factors and cytokines. These substances stimulate tumor cells, causing an increase in ROS production [31]. 3. Activation of carcinogenic signals: In the development of tumors, a variety of key carcinogenic-related proteins and downstream signaling pathways are abnormally activated, which can induce excessive ROS. For example, the continuous activation of the nuclear factor-κB (NF-κB) signaling pathway, linked to inflammation and cell survival, promotes ROS overproduction. The nuclear factor E2-related factor-2 (NRF2) acts as a crucial regulator of the antioxidant defense system, and its abnormal activation indirectly leads to ROS accumulation through redox regulatory imbalance. Furthermore, heightened activation of the phosphatidylinositol 3-kinase (PI3K) pathway is correlated with cellular proliferation and metabolic reprogramming, stimulating ROS production by changing the metabolic state of cells [32,33]. Intelligent DDS that utilize the excessive production of ROS in tumor cells as specific trigger signals have attracted extensive attention [34-36]. Currently, the ROS-responsive prodrug systems mainly include polymer-based nanocarriers [37-40], hydrogels [41,42], inorganic nanoparticle-based systems [43], and ROS-activatable prodrugs [44,45]. By coupling drug release with the ROS levels in tumor cells, these systems achieve precise therapy for tumor cells, providing a new strategy for tumor therapy [46].

This article reviewed the latest strategies of ROS-responsive anti-tumor DDS, which mainly include the following four aspects: 1. Drug-fluorophore conjugated small-molecule prodrugs with drug-fluorophore: small molecule prodrugs obtained by chemically modifying small molecule drugs are activated by ROS in tumor cells and release active parent drugs [47]. Additionally, when ROS activates the prodrug, it not only releases the active drug but also induces a change in fluorescence signal, thus enabling real-time monitoring of drug release [48]. This modification method has become widely accepted to improve the chemical and metabolic stability of drugs, as well as their water solubility or lipophilicity, extend the duration of drug action, and mitigate adverse reactions. 2. ROS-responsive polymer nanoparticles (PNPs): PNPs can be synthesized using either natural or synthetic materials, resulting in diverse structures and properties [49]. Drugs can be loaded into PNP-based DDS via encapsulation within the PNP core, embedding in a polymer matrix, chemical coupling with the polymer, or adsorption onto the PNP surface [50]. These PNPs can carry hydrophobic and hydrophilic compounds, including small molecules [51], biomacromolecules, proteins [52], and vaccines [53]. After systemic administration, PNPs preferentially concentrate at tumor locations due to the enhanced permeation and retention (EPR) phenomenon [54]. Their surface-modified target ligands enable more effective intracellular transport through receptor-mediated endocytosis. Furthermore, the ROS response unit is introduced into the polymer nanoplatform to build an intelligent DDS, which can precisely control drug release at the target in a spatiotemporal controllable manner [55]. 3. Hydrogel DDS triggered by ROS: Hydrogels consist of a three-dimensional network that results from the straightforward reaction of one or several monomers and contain a lot of water. The drug release mechanism is regulated by mesh size [56]. When the drug molecule is larger than the mesh size, it is physically encapsulated within the mesh. With the degradation of the hydrogel network, the mesh size increases, allowing the drug to diffuse freely [57]. Stimuli-responsive groups have been widely used in the development of smart hydrogels [58]. Various ROS-responsive units can induce oxidative features in polymer chains or alter their hydrophobicity to hydrophilicity through bond degradation, thereby altering the mesh size and controlling drug release [59,60]. 4. ROS-responsive inorganic nanoparticles: Inorganic nanoparticles, including gold, iron, and silica, have been utilized to create nanostructured materials, finding extensive application in drug delivery and imaging [61]. For example, free radicals on the surface of mesoporous silica (SiO_2) nanomaterials may trigger the formation of ROS through hydration reactions. In contrast, mesoporous titanium dioxide (TiO_2) has been demonstrated to be a highly effective agent for photodynamic therapy (PDT) [62]. Therefore, SiO_2 and TiO_2 have significant advantages in constructing ROS-responsive DDS. By grafting a ROS-responsive polymer onto the surface of mesoporous-structured inorganic materials, using the inorganic material as a carrier, and combining the stimulus response of the polymer, the functions of drug encapsulation and controlled release can be realized [63]. In summary, this review systematically summarized the design strategy of ROS-activated anti-tumor drug delivery platforms, demonstrating their great potential for tumor diagnosis and treatment.

The response site in ROS-sensitive prodrugs is currently divided into two categories: cleavable linking groups and non-cleavable linking groups [44]. The cleavable linking groups mainly include boronic acid and boronate (e.g., phenylboronic acid and phenylboronate) [64], thioketal [65], diselenide [66], peroxalate ester [67], vinyl disulfide, polysaccharide, and aminoacylate, among others. The non-cleavable linking groups include the chalcogen ether family (thioether, selenium ether, tellurium ether) (Figure 1). Hydrogen peroxide (H_2O_2) can oxidize the C-B bond in boronic acid [68]. In this reaction, a nucleophile engages with the boron atom, resulting in the creation of a boron anion. Following this, the phenyl group moves to the initial oxygen atom via a 1,2-shift, leading to the displacement of the hydroxyl group. The oxidation intermediate then undergoes hydrolysis with water, generating phenol and boric acid derivatives. Upon exposure to H_2O_2, the lone pair of electrons on the sulfur atom within the thioketal engages with the oxygen atom of H_2O_2, which facilitates the creation of a sulfur cation. Simultaneously, the lone pair of electrons from the nearby sulfur atom donates electrons to the adjacent carbon, causing the thioketal backbone to break and resulting in the liberation of sulfenic acid [68]. The leftover residue undergoes additional hydrolysis, eventually producing thiol and acetone, with the destruction of the thioketal structure. The initial stage of aminoacrylate's response to ROS involves singlet oxygen ($^1O_2$) directly oxidizing double bonds to form a four-membered ring structure. Subsequently, the ring collapses, producing two aldehyde groups and releasing the payload [69]. H_2O_2 acts as a nucleophile to attack the peroxalate ester and directly remove alcohol groups with R_2 groups. Subsequently, another oxygen atom undergoes a similar reaction, resulting

in the liberation of the R_1 group. This sequence of reactions eventually forms 1,2-dioxetanediones and four-membered ring intermediates, which are then converted into carbon dioxide [70]. The cleavage process of diselenide linkers begins with two molecules of H_2O_2 successively oxidizing selenium to selenium oxide. Subsequently, H_2O_2 can attack selenium atoms, leading to the creation of intermediate compounds containing hydroxyl and peroxide functional groups. This intermediate subsequently breaks down into two selenious acids by disrupting the Se-Se bond [71]. The oxidation process of selenium ether is similar to that of thioether, involving the gradual addition of oxygen to sulfur/selenium atoms, with the molecular polarity continuously increasing until it reaches its maximum value, thereby completing the transformation from hydrophobicity to hydrophilicity without breaking the chemical bond.

There is significant heterogeneity in ROS levels among different tumor tissues, and it can serve as the basis for selecting ROS-responsive groups [72]. Tumors with high ROS levels, such as glioblastoma (GBM) and esophageal squamous cell carcinoma (ESCC), can preferentially use boric acid and its ester, selenide, thioether, and thioketal responsive groups. Among them, thioketals have adjustable ROS sensitivity, and the oxidative degradation rate of thioketals can be controlled by changing the substituents [73,74]. The natural activation threshold of thioethers is relatively high, so it is necessary to use them in combination with ROS amplifiers. Boric esters exhibit unique advantages for tumors with moderate ROS levels, such as pancreatic cancer (PAAD) and

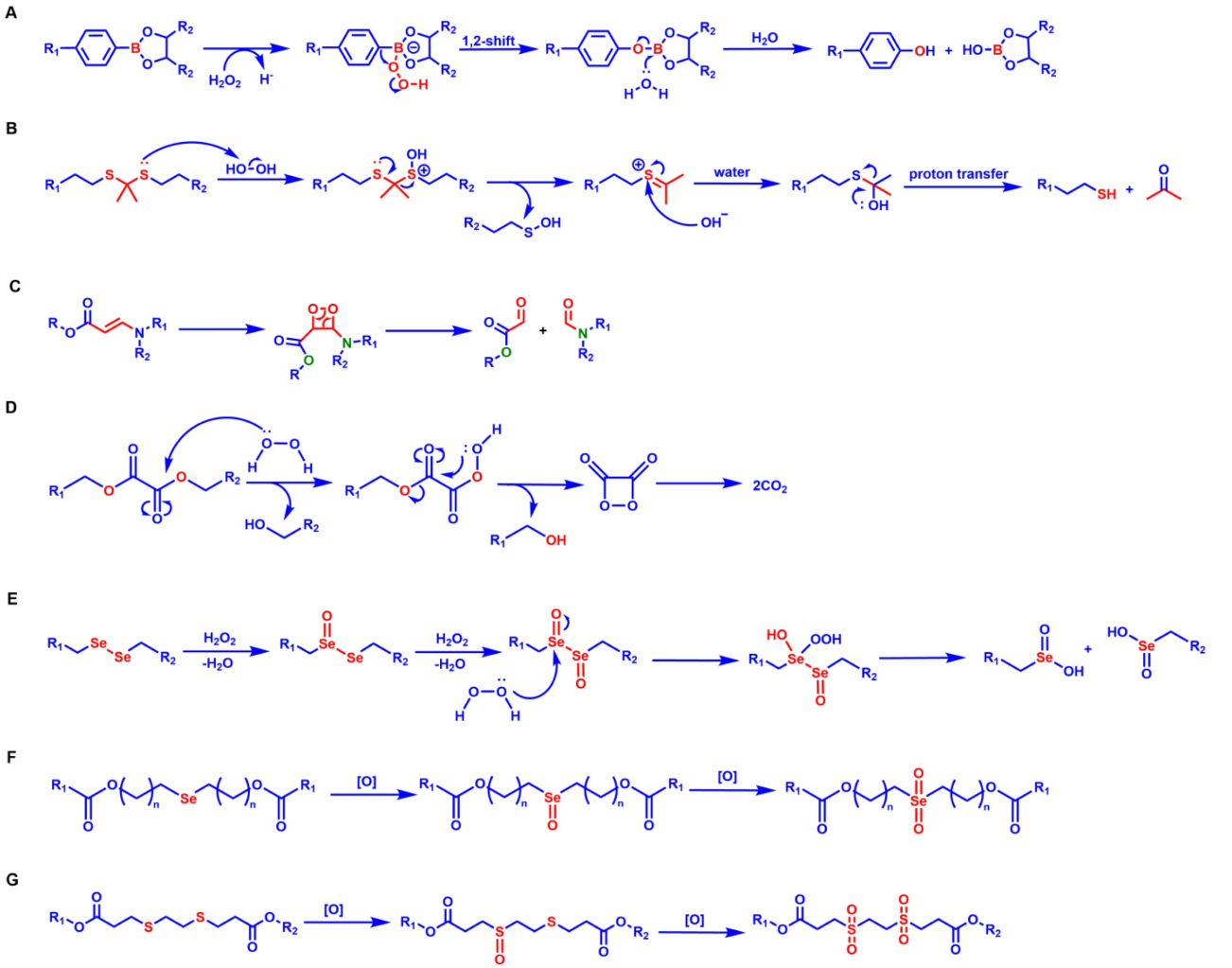

Figure 1. The response mechanisms of different ROS-responsive groups. (A) Phenylborate ester reacts with H_2O_2 under acidic conditions and undergoes hydrolysis after a 1,2-shift, generating phenol and hydroxyborate ester. (B) Thioketal undergoes oxidation, hydrolysis, and proton transfer, producing thiol and carbonyl compounds. (C) Aminoacrylate is oxidized and cleaved via a peroxide-ring intermediate, forming carboxylate ester and imide. (D) The peroxalate ester undergoes oxidation-induced rearrangement and the formation of cyclic peroxide, ultimately resulting in the release of CO_2. (E) Diselenide linkers are stepwise oxidized by H_2O_2, yielding selenium-containing oxidation products. (F) Selenium ether undergoes a two-step oxidation, first forming a selenoxide and then a selenone. (G) The thioether undergoes a two-stage oxidation, initially generating a sulfoxide and then a sulfone.

some lung adenocarcinomas (LUAD). In tumor environments that are mildly acidic (pH 6.0-6.8), boric esters can work synergistically with H_2O_2 to accelerate the hydrolysis efficiency, and the drug release rate is 5-10 times greater compared to neutral conditions (pH 7.4) [75]. For tumors with low ROS levels, such as adrenal cortical carcinoma (ACC), diselenide linkers can be selected to achieve sustained drug release and maintain long-term therapeutic concentrations. In addition, the aminoacrylate bond has a specific response to $^1O_2$ and is usually used in combination with photosensitizers under laser irradiation. The large amount of $^1O_2$ produced by the photosensitizer can effectively trigger cleavage of the aminoacrylate. This "light-controlled ROS response" mode is particularly suitable for the treatment of superficial tumors [76].

2. ROS-Activable Small Molecule Prodrugs

In the field of organic synthesis, the protection of active functional groups followed by deprotection is a common approach used to prevent adverse side effects [88]. This synthetic strategy has been applied to drug development, leading to the conception of prodrugs. Prodrug design involves conjugating specific protective groups to the active moiety of a known drug [89]. In non-healthy cells, these protective groups can be removed by enzymes or molecules, thereby restoring the pharmacological activity of the parent drug [90]. Prodrug strategies can enhance the targeting selectivity and efficacy of drugs, mitigate side effects resulting from insufficient drug solubility or low cellular uptake, and ultimately improve the overall pharmaceutical properties of drugs [91].

Small-molecule prodrugs offer several advantages, including low molecular weight, high drug loading efficiency, well-defined chemical structures, ease of monitoring their metabolic process, and feasibility of safety evaluation [92]. Their design strategy mainly involves linking the active pharmaceutical ingredient to a specific protective group (promoiety). After administration, the drug-promoiety linkage is cleaved via chemical or enzymatic reactions to activate the parent drug. In comparison to normal cells, levels of ROS in cancer cells are approximately ten times higher [93]. This disparity in concentration underpins the development of targeted prodrugs that respond to ROS. In recent years, various studies have shown that ROS can effectively serve as a trigger signal for activating prodrugs in cancer treatment, successfully applying this strategy to design ROS-responsive small-molecule prodrugs, which enable targeted drug delivery and precision cancer therapy [94] (Figure 2).

Boronic acids and their esters are commonly used as H_2O_2-responsive groups; carbon-boron bonds are cleaved via H_2O_2 oxidation, making them ideal protective moieties for the active functional groups of small-molecule prodrugs [95]. Doxorubicin (DOX) is an effective antitumor drugs in the clinic; however, its clinical application is limited due to dose-dependent cardiotoxicity caused by excessive H_2O_2 when it exerts its effect in *vivo* [96].

Table 1. Characteristics and reaction parameters of ROS-responsive groups.

ROS-responsive site	Group	Drug release process	Reaction specificity	Response concentration	Bond energy/Activation enthalpy	Refers
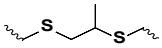	thioether	oxidation, hydrolysis	H_2O_2	50 mmol/L	272 kJ/mol	[73,74,77-79]
	thioketal				240 kJ/mol	
	diselenide	oxidation, hydrolysis	H_2O_2	0.01% H_2O_2	244 kJ/mol	[80,81]
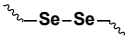	selenium ether				172 kJ/mol	
	tellurium ether	oxidation	H_2O_2	100 μmol/L	228 kJ/mol	[82-84]
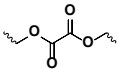	oxalate ester	nucleophilic substitution, hydrolysis	H_2O_2	10 μmol/L	$\Delta H^{\neq}$≈46.9 kJ/mol	[85,86]
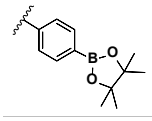	phenylboronate	Baeyer-Villiger oxidation-like rearrangement, hydrolysis, 1,6-elimination	H_2O_2	50 μmol/L	$\Delta H^{\neq}$≈90–100 kJ/mol	[87]
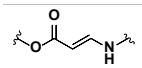	aminoacrylate	2+2 cycloaddition reaction	$^1O_2$	Producing $^1O_2$ by photosensitizer	$\Delta H^{\neq}$≈77–97 kJ/mol	[76]

Table 2. ROS-activatable prodrugs

Name	Drug	Activable group	*In vitro*/*in vivo* model	Therapeutic effect	Refs
1	DOX	Phenylboronate	4T1 H9C2	It retained the toxicity of DOX while reducing cardiotoxicity.	[98]
2 3 4	DOX	Phenylboronate	U87 MCF-7 HepG 2 MiaPaCa-2 A549	It had the highest activity in MiaPaCa-2 cells, with a prodrug conversion rate of approximately 40%.	[99]
5	Amonafide	Phenylboronic acid	MDA-MA-231 MCF-10A	It selectively inhibited DNA synthesis in tumor cells.	[100]
6 7	Crizotinib	Phenylboronic acid	H1993 H2228 RUMH	The prodrug exhibited the highest activity in H1993 cells, which had the highest ROS content.	[102]
8	Etoposide	Phenylboronate	HCT-116 xenografts in the BALB/c nude mice model	The tumor growth inhibition rate for the group administered a dose of 10mg/kg reached 46.19%.	[103]
9	β-Lap	Phenylboronic acid	Mia PaCa-2 (NQO1+) induced BALB/c mouse model	The tumor inhibition rates at doses of 20, 40, and 100 mg/kg were 54.27%, 67.52% and 71.64%, respectively.	[104]
10 11	FK886	Phenylboronic acid	293T Molt 4 PC-3	The ROS-sensitive FK866 prodrug was synthesized, which improved the targeting and efficacy of cancer treatment.	[105]
12 13	NAAF	Phenylboronate	BL-2 A2780 DU-145 Jurkat cells HDF	Prodrug 12 exhibited higher selectivity for cancer cells and had a lesser impact on normal cells.	[106]
14 15	4-FcAn	Phenylboronate	A2780	The IC_{50} values of prodrug **14** and prodrug **15** for A2780 cells were 13.8±1.0 and 8.3±0.9 μM, respectively.	[107]
16	GPX4 inhibitors	Phenylboronate	HT1080 OS-RC-2	Prodrug **16** showed stronger ferroptosis selectivity compared with GPX4 inhibitors.	[108]
17	HCPT	Thioketal bond	4T1 subcutaneous tumor-bearing mice model	The prodrug treatment group demonstrated the most significant anti-tumor effect and had relatively good safety.	[111]
18	CDOO-Me/SAHA	Thiolatic acid	A549 tumor xenograft BALB/c mice	The therapeutic effect of prodrug **18** was superior to that of the combined treatment group of CDOO-Me and SAHA.	[109]
19	F-OH-Evo	Thioether	U87 HeLa MCF-7 A549	Prodrug 19 exhibited an anti-tumor activity that was five times greater against U87 cells characterized by elevated integrin expression when compared to F-OH-Evo.	[112]
20	5-Fc	Phenylboronate	—	—	[113]
21	Fenretinide	Phenylboronate	HaCa T cells A431 SCaBER	After CPP treatment, the toxicity of prodrug **21** to different cell lines increased.	[114]
22 23	Pyrazolopyrimidinone	—	U-251MG	After being used in combination with CAP, the cytotoxicity of prodrug **22** and **23** increased by 15 times and 5 times, respectively.	[115]
24	CPT	Thioketal	A549	The apoptosis rate induced by prodrug **24** was as high as 99.6%.	[116]
25	Paclitaxel	Aminoacrylate	SKOV-3	When activated by light, the semi-inhibitory concentration values of prodrug **25** were 3.9 nM, respectively.	[117]
26	MMAE	3,5-Dihydroxybenzyl carbamate	4T1	The cell survival rate in the 4Gy+10 nM DHBC-MMAE group decreased to less than 30%.	[110]

H_2S is a cardioprotective agent with anticancer activity [97]. Lukesh III *et al.* [98] synthesized prodrug **1** (Figure 3) by connecting boronate with DOX via the structure of carbonyl sulfide. H_2O_2-activated prodrug **1** within the TME and simultaneously released DOX along with H_2S. H_2S directly scavenged ROS, enhanced the endogenous antioxidant system, and alleviated DOX-induced cardiotoxicity. Compared with DOX, prodrug **1** reduced apoptotic effects on cardiomyocytes by releasing H_2S, and the dose of prodrug **1** did not impede Nrf2 activation or cardiomyocytes' HO-1 expression, thus minimizing cytotoxicity. Therefore, prodrug **1** had significant potential as an alternative to DOX for reducing cardiotoxicity while retaining antitumor efficacy.

The effect of the prodrug formed by combining DOX with arylboronic acids on different cell lines varies significantly, which affects its potential for entry into clinical trials. Therefore, it is crucial to identify tumor cell lines sensitive to varying subtypes of arylboronic acid prodrugs. Labruère *et al.* [99] synthesized a series of H_2O_2-sensitive prodrugs, including non-substituted boronate prodrug **2**, fluorinated phenol analogs prodrug **3**, and furan-substituted boronate prodrug **4** (Figure 3). They evaluated the H_2O_2-induced activation efficiency and DOX release efficiency in different tumor cell lines. The results showed that prodrug **2** exhibited the best anti-tumor activity and the highest selective activity against pancreatic cancer cells, with the recovery rate

of the active drug reaching 67% of the activity of free DOX. The effect of prodrug **2** was comparable to that of similar free DOX in the MiaPaca-2 tumor model. Yin *et al.* [100] developed an H_2O_2-responsive theranostic prodrug **5** based on amonafide (AMF) (Figure 3), which could be used to compare and quantify the H_2O_2 levels of different cells. Experimental results confirmed that the intracellular H_2O_2 concentration was positively correlated with the anticancer activity of prodrug **5**.

Crizotinib is a tyrosine kinase inhibitor. The 2-aminopyridine functional group in its structure can interact with the amino acids in the ATP-binding sites of the three targeted kinases (Anaplastic Lymphoma Kinase, cellular Mesenchymal-epithelial Transition factor, and ROS proto-oncogene 1, receptor tyrosine kinase), which is regarded as an ideal structural unit for prodrug modification [101]. Kowol *et al.* [102] conjugated the 2-aminopyridinium moiety of crizotinib to phenylboric acid via a covalent linker to prepare prodrugs **6** and **7** (Figure 3). Boronic acid as a ROS-responsive trigger fragment, and the 2-aminopyridinium moiety as the key site for target kinase binding. The study found that H_2O_2 activated prodrug **6** more easily, and the activity level of prodrug **6** was significantly and positively correlated with the intracellular H_2O_2 concentration. Therefore, the strategy of converting crizotinib into a prodrug can reduce systemic side effects while improving tissue selectivity for tumor cells.

Coumarin is commonly used as a tracking agent when the prodrug is released, especially for the prodrugs modified with boronic acid groups. Yu *et al.* [103] synthesized peroxide-sensitive prodrug **8** (Figure 3) by conjugating etoposide to phenylboronate via a coumarin linker. Etoposide is a topoisomerase II inhibitor that induces the death of tumor cells by creating complexes involving topoisomerase II and DNA. Although etoposide is widely utilized as a first-line chemotherapy, its use in clinical settings is hampered by cardiac toxicity, hematological toxicity, and gastrointestinal toxicity. Prodrug **8** was specifically triggered in cancer cells to release etoposide, and it exhibited similar anti-tumor

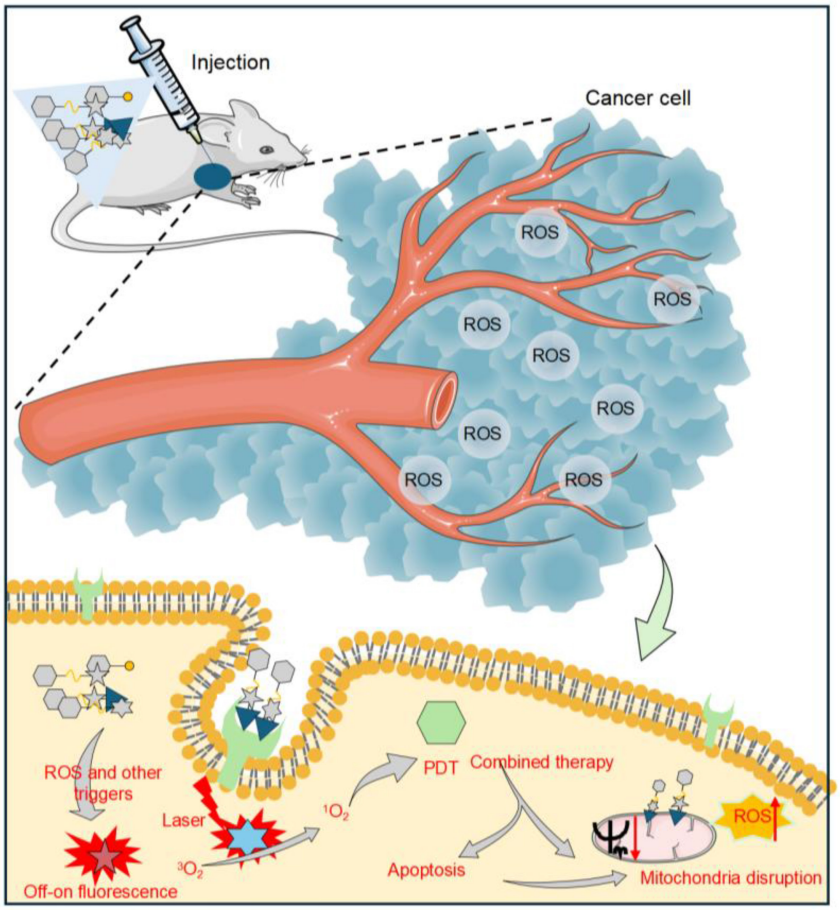

Figure 2. A schematic representation of how small-molecule prodrugs function in the treatment of tumors. After administration, the prodrug is transported to the tumor location and activated within the TME, which is marked by elevated levels of ROS. The fluorophores integrated into the prodrug exhibit an "on-off" fluorescence response during activation and functional depletion, facilitating the real-time monitoring of prodrug activation and its therapeutic effects. Under laser irradiation, the photosensitizer portion within the prodrug generates $^1O_2$. $^1O_2$ works synergistically with chemotherapeutic drugs released by activated prodrugs, destroying mitochondrial function and ultimately inducing apoptosis of cancer cells. Meanwhile, targeting groups in the prodrug allow for specific recognition and binding to highly expressed receptors on tumor cells, enhancing the delivery accuracy and therapeutic specificity.

activity to that of etoposide, along with enhanced safety and reduced toxicity. Due to the presence of coumarin, the activation of prodrug **8** resulted in a notable rise in fluorescence intensity within tumor cells; therefore, prodrug **8** was expected to be a safe and effective anticancer chemotherapeutic agent.

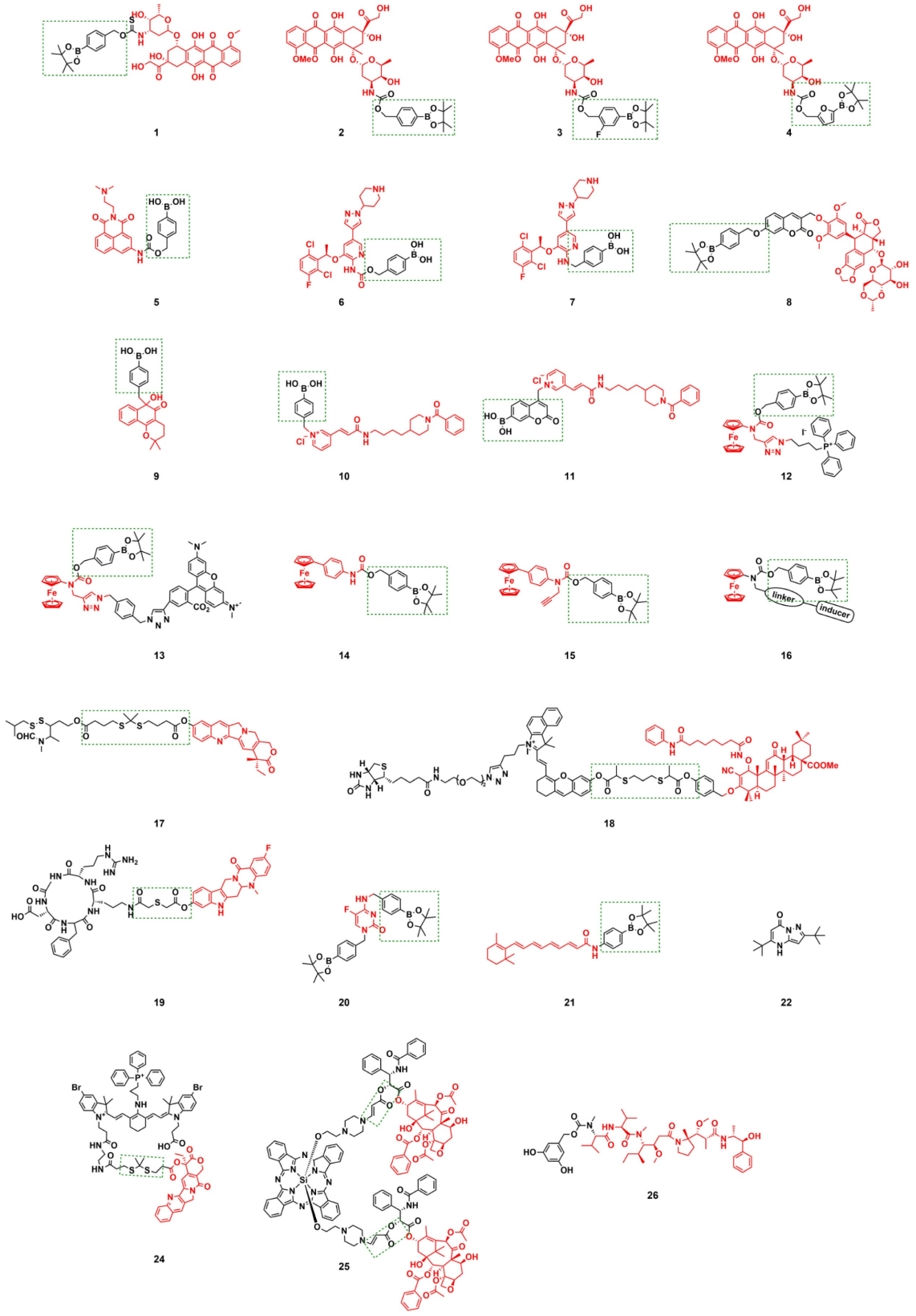

Figure 3. The chemical architecture of prodrugs that respond to ROS. The prodrug depicted in the figure enables site-specific activation and drug release in ROS-enriched TME by coupling the chemotherapy drug (highlighted in red) with a ROS-reactive group (in the green box).

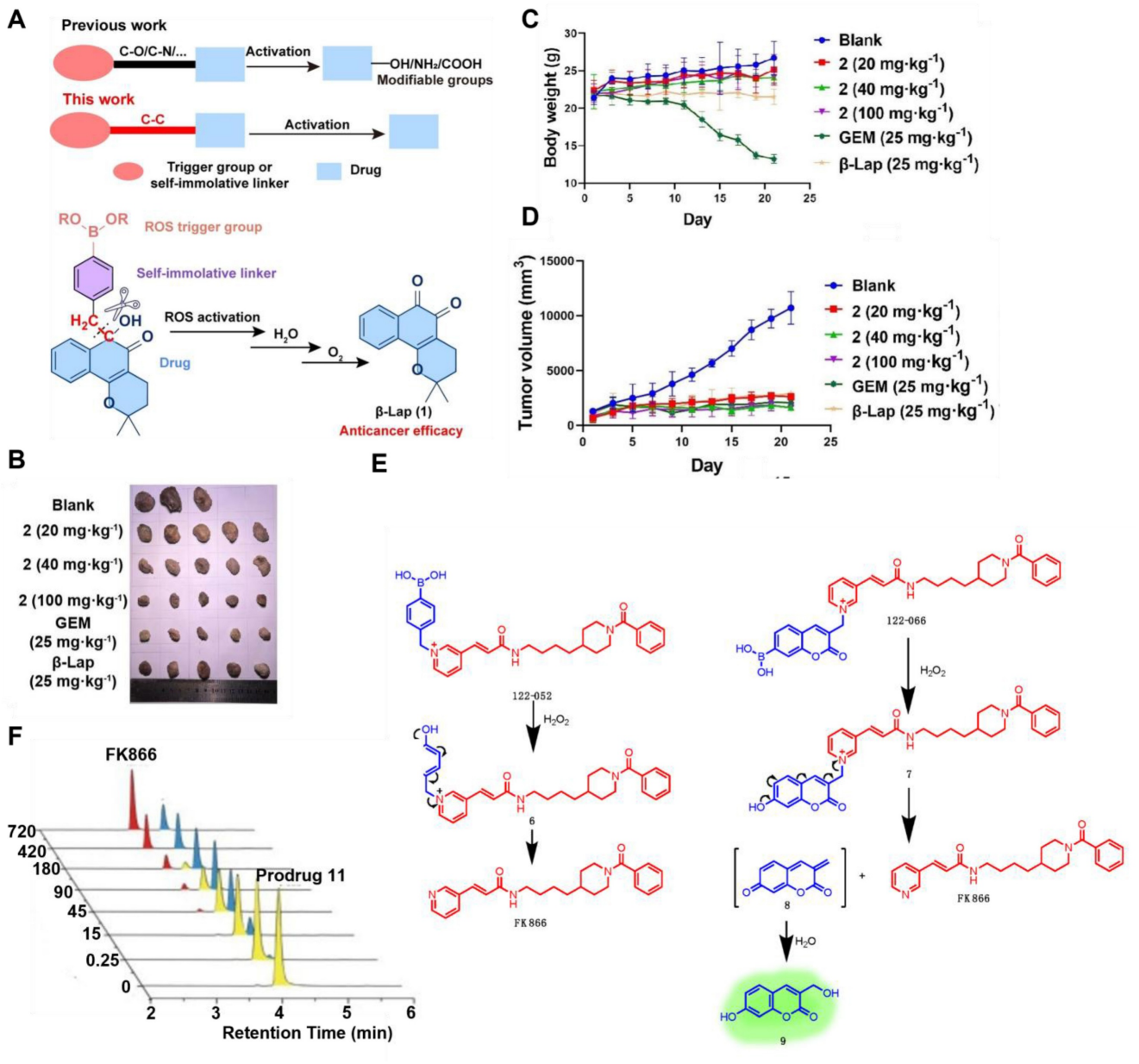

Figure 4. (A) A new prodrug strategy for activating ROS-reactive anticancer prodrugs through C-C bond cleavage. (B) Tumor image after compound treatment of Mia PaCa-2 xenograft in nude mice. (C) The weight of the tumor during treatment. (D) The volume of the tumor after treatment. Produced with permission [104]. Copyright 2022, Wiley-VCH GmbH. (E) Diagram of the process of FK866 release from the prodrug **11**. (F) Conversion of prodrug **11** to FK866 monitored by HPLC. Reproduced under terms of the CC BY 4.0 license [105]. Copyright 2020, by Jiang *et al.*

Current boronate prodrugs face substantial challenges in altering active functional groups within parent drugs. Zhang *et al.* [104] proposed a prodrug activation strategy based on C-C single bond cleavage and successfully designed a β-lapachone (β-Lap)-based prodrug **9** (Figure 3). Under the induction of ROS, the C-C bond in the prodrug structure was rapidly cleaved, releasing the parent drug β-Lap. β-Lap exerted anticancer effects through an effective redox cycle mediated by NAD(P)H: quinone redox reductase 1 (NQO1) and exhibited significant selectivity for NQO1-overexpressing tumor cells (Figure 4A-D). This method offered a new perspective on the exploitation of prodrugs from traditional drugs.

Nicotinamide phosphoribosyltransferase (NAMPT) is a rate-limiting enzyme widely present in tumor cells, has the potential to be targeted by inhibitors for cancer therapy. However, the dose-limiting toxicity of them has hindered their clinical application. Jiang *et al.* [105] reported NAMPT prodrugs **10** and **11** (Figure 3), which could be activated by ROS, and the toxicity was significantly reduced in normal cells compared to their parent NAMPT inhibitor. Moreover, because prodrug **11** contained a coumarin fluorophore, its fluorescence

signal changed when the parent drug was released from it under H_2O_2 activation (Figure 4E-F).

Delivering drugs to organelles lifts the anticancer effect. Mokhir *et al.* [106] synthesized prodrugs **12** and **13** (Figure 3) with mitochondrial targeting function by coupling N-alkylamine ferrocene (NAAF) to an alkyl triphenylphosphine (TPP) carrier and N,N,N′N′-tetramethylrhodamine, respectively. Prodrugs could form p-quinone methyl, CO_2, intermediates 1, 2, 3, and drugs in a medium containing a large amount of ROS (Figure 5A). Experiments showed that both prodrugs could accumulate and be activated directly in the mitochondria of tumor cells. The mechanism of action involved weak ROS produced by NAAF modulating mitochondrial membrane potential (a process facilitated by TPP-mediated mitochondrial targeting). This discovery opened new opportunities for the advancement of cancer research and the development of treatments. However, aminoferrocene-based drugs were unstable under oxidative conditions, which led to their easy inactivation in tumor cells. Subsequently, the team selected 4-ferrocenyl aniline (4-FcAn), which was more stable than ferrocenylamino-ferrocene (AF), for the synthesis of prodrugs **14** and **15** [107] (Figure 3). Under aerobic conditions, 4-FcAn could remain stable in buffer solution for an extended period and facilitated the production of more reactive OH• from H_2O_2 via a Fenton-like reaction. Prodrugs **14** and **15** were superior to prodrugs **12** and **13** in terms of ROS-generating capacity and antitumor efficacy. Wang *et al.* [108] designed and synthesized boronate prodrugs of NAAF, and conjugated these prodrugs with Glutathione Peroxidase 4 (GPX4) inhibitors (RSL3, ML162, and ML210) to form prodrug **16** (Figure 3). The prodrug **16** exhibited higher ferroptosis selectivity and more potent anticancer activity, thereby addressing the selectivity and toxicity issues associated with GPX4 inhibitors.

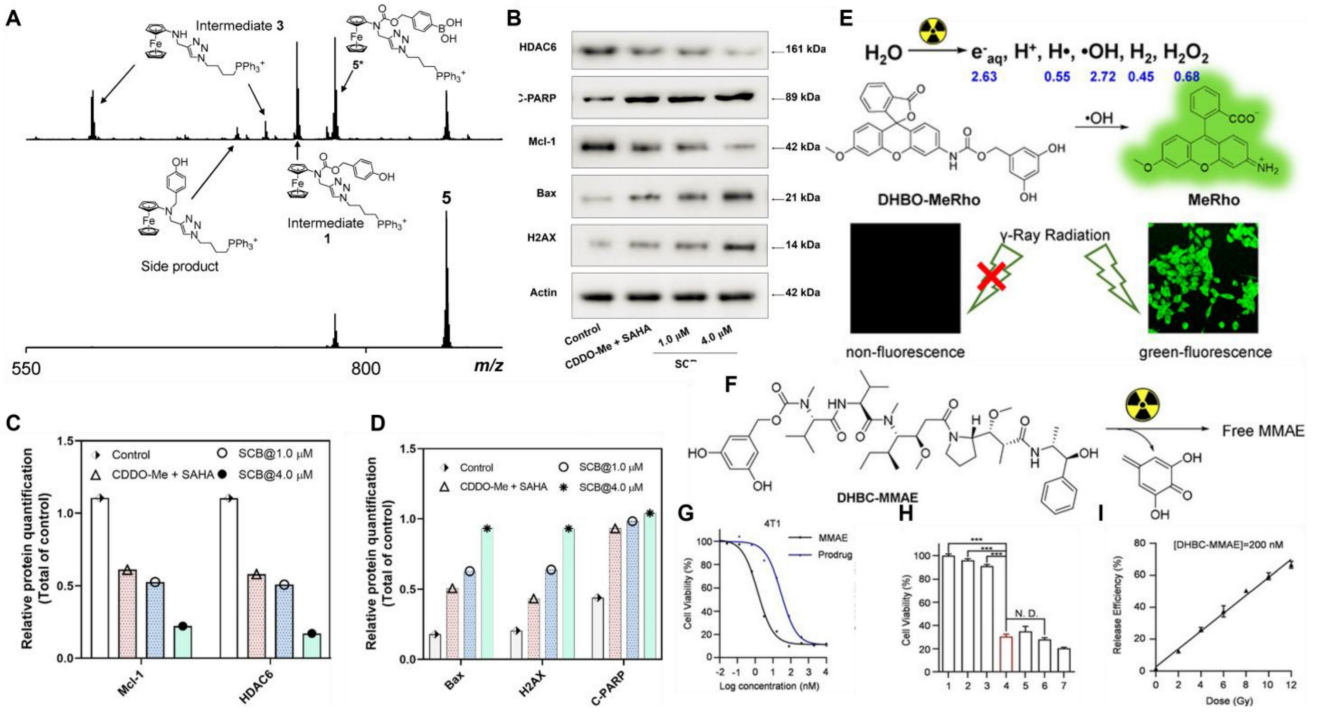

Figure 5. (A) Mass spectra (obtained through electrospray ionization (ESI) in positive mode) for the prodrug **12** (at a concentration of 40 μM in N,N-dimethylformamide DMF/CH_3CN/H_2O, in a ratio of 1/10/90, v/v/v) were recorded with H_2O_2 present (35 mM, top) and absent (bottom) at a temperature of 22°C. Reproduced under terms of the CC BY 4.0 license [106]. Copyright 2020, by Mokhir *et al.* (B) Impacts of 1.0 μM CDDO-Me combined with 1.0 μM SAHA and SCB (1.0 and 4.0 μM), on the expression of proteins associated with apoptosis and anti-apoptosis in A549 cells. (C, D) Quantitative assessment of Mcl-1, HDAC6, Bax, H2AX, and C-PARP in various treatment conditions. Reproduced with permission [109]. Copyright 2022, American Chemical Society. (E) A schematic diagram showing the selective and effective removal of DHBC as a masking group by OH• generated by external radiation. (F) Chemical structure of the MMAE prodrug. (G) The cell viability of 4T1 cells after co-incubation with MMAE and prodrug **26**. (H) MMAE in vitro controlled-release cell viability assay ([prodrug **26**]=10 nm, n=5, double-tailed unpaired Student's t-test, ***P<0.001). (I) Drugs with radiation dose gradient release ([prodrug **26**]=200 nm, Co-60 as the γ radiation source, 1 Gy/min). All samples were incubated for 2 hours before analysis. Reproduced with permission [110]. Copyright 2022, Wiley-VCH GmbH.

Different ROS or GSH levels in different regions or stages of tumor tissues result in heterogeneous redox states, leading to partial activation of the ROS-responsive prodrug. To further improve the activation level, Wu *et al.* [111] conjugated GSH-sensitive thiamine disulfide (TDS) to 10-hydroxycamptothecin (HCPT) through a thioketal bond to obtain prodrug **17** (Figure 3). TDS reacted with GSH to generate intermediates with substantial positive charges, which could effectively remain in tumor cells and prevent efflux via charge-mediated interactions. High levels of ROS subsequently activated this intermediate, releasing HCPT. This dual-responsive design optimized the targeting ability of prodrug 17. Ling *et al.* [109] synthesized ROS/GSH dual-responsive prodrug **18** (Figure 3) using bis(sulfanediyl) dipropionate. This prodrug could attenuate the toxicity of suberoylanilide hydroxamic acid (SAHA) and C-28 methyl ester of 2-cyano-3,12-dioxoolen-1,9-dien-28-oic acid (CDDO-Me) in normal tissues, thereby reducing their related side effects and enabling a synergistic approach to combination chemotherapy (Figure 5B-D). Furthermore, prodrug **18** was equipped with a biocompatible fluorescent dye, indocyanine green (ICG) (Figure 6), and a biotin targeting moiety. This design increased the proportion and kinetic rate of prodrug activation in tumor tissues, providing a novel safety framework for accurate diagnosis and guidance for tumor resection and selective combination therapy. Hu *et al.* [112] synthesized prodrug **19** (Figure 3), which attaches the αvβ3-targeting cyclic peptide cRGD to 3-fluoro-10-hydroxy-Evodiamine (F-OH-Evo) via a thioether bond, allowing the swift release of the parent drug while exhibiting improved anti-tumor migration activity.

The prodrugs above were designed based on the higher ROS levels in the TME. Additionally, exogenous stimuli such as light, ultrasound, and heat can either activate prodrugs directly or induce ROS production in the TME, thereby facilitating ROS-mediated drug release. Wende *et al.* [113] synthesized 5-fluorocytosine prodrug **20** incorporating an aryl boronate moiety and utilized cold physical plasma (CPP) to generate ROS (Figure 3). They found that CPP triggered the ROS reaction of prodrug **20,** releasing the drug (Figure 5E-G). Using this strategy, the same team [114] also synthesized prodrug **21** (Figure 3), in which the aryl boronate group was used to mask the highly reactive hydroxyl group of fentretinoin, reducing its chemical reactivity, improving its aqueous solubility, and enhancing its selectivity toward tumor cells. CPP-induced ROS and RNS triggered the release of fentitic acid from prodrug **21**, reducing adverse side effects. These results indicated that CPP-reactive prodrugs are valuable for further study.

Similar to CPP, cold atmospheric plasma (CAP) can regulate the source of ROS and RNS, thereby promoting drug release. Curtin *et al.* [115] synthesized pyrazolopyrimidinone prodrugs **22** and **23** (Figure 3) and combined the prodrugs with CAP to study the anti-tumor effect. The combination of **22** and **23** with low doses of CAP demonstrated cytotoxicity that was 15 and 5 times greater in U-251MG cells, respectively. The result displayed that the combination of CAP and pyrazolpyrimidinone could activate prodrugs locally in tumors, thereby minimizing the effects on other tissues and providing an innovative strategy for creating pyrazolpyrimidinone prodrugs.

Thioketal bonds can be selectively cleaved by H_2O_2 and exhibit strong modifiability, making them ideal connecting groups for the activation of ROS. Gao *et al.* [116] utilized thioketal bonds to link the chemotherapeutic drug camptothecin (CPT) with the photosensitizer TPP-NIR (Figure 6), introducing a mitochondrial targeting group, TPP, to obtain the ROS-activated anticancer prodrug **24** (Figure 3). After the prodrug entered the mitochondria of the tumor cells, TPP-NIR produced $^1O_2$ under light irradiation, significantly increasing the level of mitochondrial reactive oxygen species (mtROS). High concentrations of ROS broke the thioether bond, releasing CPT and initiating mitochondrion-mediated apoptosis. Compared to previously reported ROS-activated CPT prodrugs, prodrug **24** leveraged photodynamic therapy (PDT) to achieve superior spatiotemporal control in cancer treatment, thereby minimizing damage to healthy tissue. Using the same strategy, You *et al.* [117] developed prodrug **25** by linking paclitaxel to the fluorescent photosensitizer phthalocyanine (Pc) (Figure 6) with a $^1O_2$-cleavable aminoacrylate linker (Figure 3), which produced $^1O_2$ under far-infrared light irradiation, triggered direct photodynamic damage, and released paclitaxel specifically at the irradiation site. In *vitro* experiments with SKOV-3 ovarian cancer cells demonstrated potent cytotoxicity (IC_{50} = 3.9 nM). This innovative approach combined PDT with site-specific paclitaxel chemotherapy, presenting a hopeful method for eliminating cancer.

In addition to extensively exploring the synergistic application of ROS-responsive prodrugs with PDT, many studies have reported their combined regimens with radiotherapy. The challenges associated with using PDT for deep tumors have been addressed due to the profound ability of radiation to penetrate deep tissues. As a masking group, 3,5-dihydroxybenzyl carbamate (DHBC) could be specifically and effectively removed by OH•

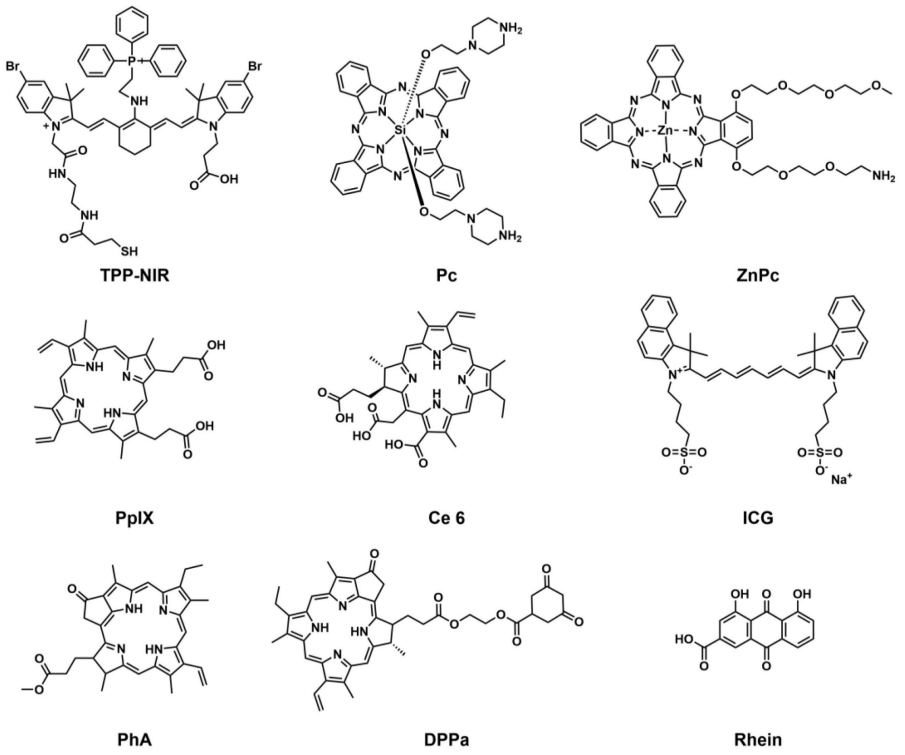

Figure 6. The chemical structure of photosensitizers and sonosensitizers in ROS-reactive tumor treatment systems. They can produce ROS under light or ultrasonic stimulation. Both are key components for amplifying ROS levels in the TME or triggering ROS-mediated activation of prodrugs.

generated by external radiation (Figure 5E). Liu *et al.* [110] synthesized the radiation-activating prodrug **26 (**Figure 3**)**. At the clinical standard dose of 4 Gy, the release of MMAE dramatically reduced the activity of 4T1 cells, demonstrating high in *vitro* cleavage efficiency and potential therapeutic effects (Figure 5F-I).

3. ROS-Activatable Polymeric Nanoprodrugs

Small-molecule prodrugs activated by ROS show significant potential for tumor treatment because of their specific activation in the TME. However, these compounds have significant limitations: their unsatisfactory pharmacokinetic properties make it difficult to achieve targeted and precise drug delivery, and rapid metabolism in the body is also quite prominent. These deficiencies significantly limit their therapeutic efficacy and clinical application. In contrast, the physical properties (such as morphology and size) of polymeric nanoparticles can be precisely controlled by regulating the hydrophilic-lipophilic balance and optimizing the preparation process, thereby effectively improving their biological distribution in *vivo* [52]. Based on the above context, scientists have successfully developed ROS-activated polymer nanomedicine systems for cancer treatment [40]. After systemic administration, these systems concentrate at tumor locations and dispense medications precisely at the target site via a spatiotemporally controllable mechanism [118]. By introducing targeted ligands to modify the surface of nanoprodrugs, the intracellular delivery efficiency of drugs can be further enhanced *via* receptor-mediated endocytosis [40,119]. This innovative design is anticipated to address the shortcomings of conventional small-molecule prodrugs. In the past few years, notable advancements have been achieved in the creation of ROS-responsive polymer nanomedicines. This section systematically classifies these nanomedicines into four categories based on molecular design principles and response mechanisms: I. ROS-responsive groups are introduced into the polymer to construct ROS-responsive PNPs, which are then used to encapsulate therapeutic drugs. II. The polymer is linked to the drug via a ROS-responsive connector, and polymer nanoprodrugs are constructed. III. Stimulus-responsive nanomaterials can be used to encapsulate ROS-responsive small-molecule prodrugs, which are released under multiple stimuli, effectively avoiding the release of chemotherapeutic drugs in normal tissues while retaining the advantages of nanoprodrugs. Strategy IV is similar to Strategy III, except that it utilizes iron-coordinated nanocarriers to encapsulate small-molecule prodrugs, thereby constructing polymer nanocarriers (Figure 7).

3.1. Introducing ROS-responsive groups into polymers to construct polymer nanoprodrugs

Sulfur, a typical non-metallic element, is prone to oxidation. This characteristic is also reflected in sulfur-containing polymers, which are prone to oxidation in ROS-rich environments. For example, sulfur atoms in thioethers are easily oxidized by ROS to form sulfoxide groups. This transformation often changes materials from hydrophobic to hydrophilic. The significantly enhanced water solubility enables DDS to achieve controllable drug release in ROS-enriched environments [120]. Based on this principle, Liu *et al.* [121] developed the copolymer PEG-PPMT with pH and ROS response properties via amino groups and sulfide moieties. The copolymer self-assembled into nanocarriers in water and successfully encapsulated the chemotherapy drug, docetaxel (DTX). Experiments showed that the carrier structure disintegrated when sulfides were oxidized to sulfoxides in the TME, facilitating the specific release of DTX. This intelligent delivery system demonstrated excellent tumor-suppressing effects in *vivo* (Figure 8E-G), particularly showing precise and targeted therapeutic potential in tumors with elevated ROS levels. In a similar research direction, Wang's group [122] designed sulfide-based block copolymers based on polyethylene glycol (PEG) and poly (2-methyl-5-sulfostyrene). This amphiphilic polymer formed ROS-responsive nanoparticles via self-assembly (Figure 8A-E). Cell experiments have shown that nanocarriers can release loaded drugs in response to intracellular ROS.

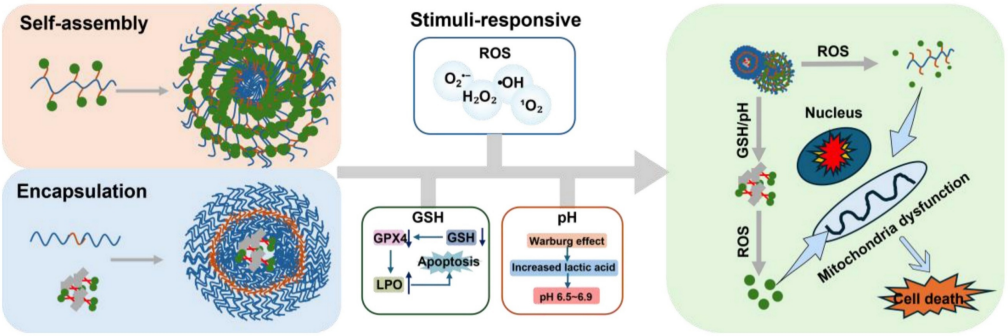

Figure 7. A schematic illustration depicting how ROS-reactive polymer nanomedicines function in the treatment of tumors. This figure systematically describes the multi-step process of polymer nanoprodrugs, including self-assembly, tumor targeting, time-triggered and activated release, controlled drug release, and synergistic anti-tumor treatment, to achieve targeted and efficient tumor elimination.

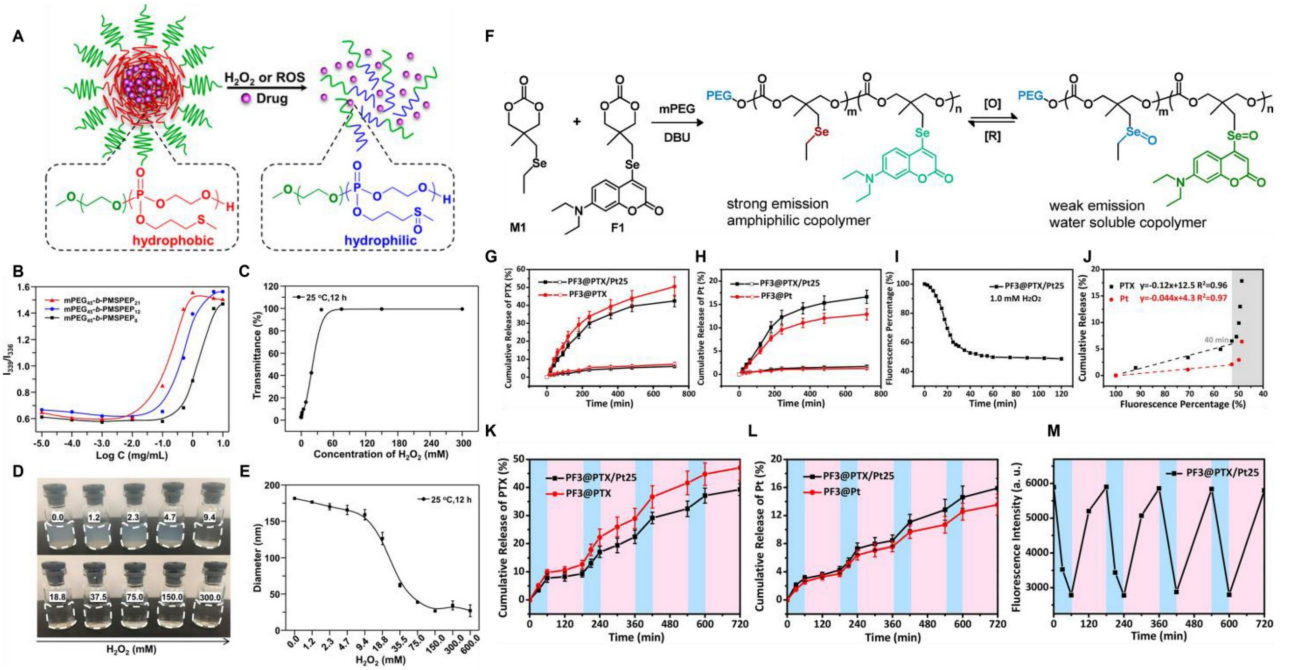

Figure 8. (A) mPEG-*b*-PMSPEP undergoes ROS- or H_2O_2-triggered cleavage to release the encapsulated drug. (B) Intensity ratio (I_{339}/I_{336}) of mPEG-*b*-PMSPEP at different concentrations. (C) Oxidation response behavior of $mPEG_{45}$-*b*-$PMSPEP_{21}$ when exposed to varying amounts of H_2O_2. (D) Images of nanoparticles incubated in H_2O_2 solutions of different concentrations. (E) Diameter changes of nanoparticles following co-incubation with varying concentrations of H_2O_2. Reproduced with permission [122]. Copyright 2019, American Chemical Society. (F) The synthesis process of fluorescent copolymers and their reversible redox reaction transformation. (G, H) 1.0 mg/mL PF3@PTX/Pt25 nanoparticle in PBS (pH 7.4, 10 mM) with (solid symbol) or without (empty symbol) H_2O_2 (1.0 mM), PTX's (G) and cisplatin's (H) cumulative release at 37°C. (I) variation of the

percentage of fluorescence of PF3@PTX/Pt25 over time. The data is normalized relative to the initial strength. (J) Accumulative release of drug from PF3@PTX/Pt25 plotted against fluorescence percentage. (K, L) At 37°C, the cumulative release of PTX (K) and cisplatin (L) from PF3@PTX/Pt25 (1.0 mg/mL) in PBS (pH 7.4, 10 mM) was achieved through four REDOX cycles. The results are expressed as mean ± standard deviation. (M) Variation of fluorescence intensity over time. The data is normalized relative to the initial strength. Oxidation, 1.0 mM H_2O_2, 60 min; Restore, 1.0 mM VC, 120 min. Reproduced with permission [124]. Copyright 2019, American Chemical Society.

Table 3. ROS-activatable polymeric nanoprodrugs.

Name	Drugs	Activable groups	*In vitro*/*in vivo* model	Therapeutic effect	Refs
DTX/PEG–PPMT	DTX	Thioether	A549 tumor xenograft BALB/c mice	Free DTX, DTX-loaded PEG-PPMT-11% PDL, and DTX-loaded PEG-PPMT-28% PDL nanoparticles inhibited tumor growth by 39%, 95%, and 93%, respectively.	[121]
MS-NP/Ce6&PTX	PTX	Thioether	MDA-MB-231	Combined phototherapy yielded the highest anti-cancer efficacy for MS-NP/Ce6&PTX.	[122]
PDA-Dox-Pc-QRH	DOX	Thioketal	A431 tumour-bearing mice	Laser-irradiated PDA-Dox-Pc-QRH eliminated tumors in approximately 10 days.	[123]
PF@PTX/Pt	PTX/Pt	Selenide	MDA-MB-231 HBL-100	PF@PTX/Pt showed concentration-dependent cytotoxicity against MDA-MB-231 and was not effectively activated in HBL-100 cells.	[124]
2BOH-TOS/DOX	DOX	boronate	MCF-7 MCF-7/ADR spheroids	The tumor growth rates observed in MCF-7 spheroids for Free DOX, 2BOH-TOS/NP, and 2BOH-TOS/DOX were -0.26, -0.31, and -0.51, while in MCF7/ADR spheroids, the rates were 1.84, 0.24, and -0.19, respectively.	[125]
mPEG-ROS-DOX	DOX	Thioketal	Balb/c mice bearing subcutaneous HepG2 tumors	Compared with mPEG-ROS-DOX, DOX had a more effective inhibitory effect on tumor growth; however, weight loss occured, with a maximum reduction rate of up to 20%.	[126]
Lapa@NPs	CPT	Thioketal	4T1 tumor-bearing mice with the tumor	On the 21st day, the tumor volume in the PBS treatment group rose significantly to 12.1 times, whereas the increase in tumor volume for the Lapa@NPs group was only 3.3 times.	[129]
TA-CA-Prodrug	PTX	Thioketal	4T1 tumor-bearing mice	The inhibition rates of tumor growth for the PTX group and the TA-CA-Prodrug group were 21.9% and 58.9%, respectively.	[130]
PTCD@B	DOX	Thioacetal	L929 4T1	PTCD@B has low toxicity to normal cells but shows significant cytotoxicity to 4T1 cells.	[131]
PEG-TK-DOX/PhA	DOX	Thioketal	CT 26 tumor-bearing mice	The group subjected to laser irradiation demonstrated a notable reduction in tumor size when contrasted with the non-irradiated group and the group receiving PBS injections.	[132]
Ce6@PPE-TK-DOX	DOX	Thioketal	Mice bearing MDA-MB-231 tumors	The Ce6@PPE-TK-DOX NPs(L+) group exhibited the highest anticancer efficacy.	[133]
PSPC NAs	CTX	Thioketal	Balb/c nude mouse model of A375 human melanoma	It had the potential to greatly reduce tumor growth while exhibiting low systemic toxicity and a high level of safety. The maximum tolerable dosage was notably greater than that of unbound medications.	[134]
DPPa NPs	CL	Thioketal	4T1 tumor-bearing mice	The tumor suppression rate of the DPPa NPs+ laser group was 85.8%.	[135]
ICG-PBT@NMPs	TPZ	Phenylboronate	4T1 tumor-bearing mice	ICG-PBT@NMPs had successfully achieved tumor inhibition through continuous bioadhesion.	[136]
RP-NPs	GEM	Thioketal	HeLa tumor-bearing nude mice	The weight of the tumor in the RP-NPs+US group was roughly one-third of that observed in the control group, demonstrating a therapeutic effect that outperformed that of RP-NPs used on their own.	[137]
ZnPc@Cur-S-OA	Cur	Thioketal	BALB/c mice inoculated with B16F10 cells	The ZnPc@Cur-S-OA + laser group showed significant tumor volume and load suppression effects after treatment.	[138]
Pro-5-FU@cLANCs	Pro-5-FU	Phenylboronate	A549 xenograft tumor model	Pro-5-FU@cLANCs achieved a tumor suppression rate of 73.1% and a survival rate of 80%.	[144]
$^{SS}CB_{EPB+K}$	DOX	Phenylboronate	orthotopic BC xenograft models in female C57BL/ 6 J mice	$^{SS}CB_{EPB+K}$ exhibited a similar performance to free EP in inhibiting tumor growth, with an extended survival time of over 60 days.	[145]
PHI@B/L	Lap/BDOX	Hydrazone bond/Phenylboronate	4T1 tumor-bearing mice	In comparison to the free DOX group, the PPHI@B/L group exhibited both the lowest tumor weight and volume, as well as a notable enhancement in tumor suppression and survival rates.	[146]
HCAG	GEM	Thioacetal	4T1 tumor-bearing mouse model	HCAG exhibited excellent in vivo anti-tumor effects at a dose of 10 mg/kg, with extremely low systemic toxicity.	[147]
ProCPT@P3	CPT	Phenylboronate	4T1 tumor model	Compared to CPT, ProCPT@P3 exhibited an enhanced inhibitory effect on tumor growth and a significantly reduced proliferation rate of tumor cells.	[148]
P-NM-Lapa	NM/Lapa	Phenylboronate	xenograft mouse models of HeLa cells	The tumor volume in mice treated with the P-NM-Lapa combined treatment was significantly reduced.	[149]
PDOX	DOX	Diselenide	HepG2 L02	PDOX demonstrated a toxicity that varies with dosage in HepG2 cells, resulting in a cell survival rate of 51%. Conversely, it displayed favorable cytocompatibility with LO2 cells.	[150]
PSD-Fc	PTX/DHA	Thioether	4T1 tumor-bearing mice	The mean tumor volume on day 22 was 1536 mm^3 and 562 mm^3 for mice administered with PBS and PSD-Fc, respectively.	[156]
$^{TK}NP_{DHA}$-Fc	PTX/DHA	Thioketal	4T1 tumor-bearing BALB/c mice	The average tumor mass of the $^{TK}NP_{DHA}$-Fc group was 0.16±0.03 grams, which was 0.61 times and 0.42 times lower than that of the control groups NP_{DHA} and $^{TK}NP_{DHA}$, respectively.	[155]
SN38-CA@FC	SN38	Thioacetal linker	xenograft LLC-bearing C57BL/6 mouse model	In the control group, the tumor volume rose to approximately 1250 mm^3, while the tumor volume for SN38-CA@FC fell to 110 mm^3.	[157]

Similarly, polymers with ROS-responsive groups have found wide application in tumor treatment. ROS at the tumor site can break thioketal bonds, thereby facilitating drug release. Ng *et al.* [123] first obtained a dimer by connecting 3,4-dihydroxy-L-phenylalanine to thiol groups (Figure 6 L-DOPA dimer). This dimer underwent self-polymerization in the presence of DOX to obtain DOX-containing polydopamine (PDA) nanoparticles, which were coupled with ZnPc photosensitizers and heptapeptides (QRH) capable of targeting the epidermal growth factor receptors to prepare the ROS-responsive polydopamine nanoparticles. After entering the cells through receptor-mediated endocytosis, these nanoparticles gradually degraded in the presence of ROS, releasing DOX and Pc molecules (Figure 8B-D). Under light exposure, they could generate more ROS, further promoting the degradation of nanoparticles and drug release, thereby forming a synergy between chemotherapy and photodynamic therapy. In nude mice with overexpression of EGFR-bearing tumors, PDA-Dox-Pc-QRH achieved tumor-targeted delivery, effectively inhibited tumor growth under light, and even resulted in complete tumor ablation.

As a sulfur homolog, selenium can also undergo specific oxidation reactions in the ROS microenvironment. The hydrophobic monoselenium group is oxidized to a hydrophilic selenosulfone group, which triggers drug release. Additionally, diselenide bonds can undergo oxidative breakage to form seleninic acid. This unique oxidative response mechanism offers a novel approach for tumor-targeted therapy. Li *et al.* [124] synthesized ROS-responsive nanoparticles PF using selenium-containing amphiphilic block copolymers and co-loaded cisplatin and paclitaxel (PTX) as chemotherapy drugs while introducing coumarin-based fluorescent groups (Figure 9 PF). The coordination effect of Se-Pt significantly improved the stability of the drug-loaded system while maintaining its high sensitivity to oxidative microenvironments. By leveraging the reversible transformation characteristics of selenide/selenosulfone in the selective redox cycle, simultaneous monitoring of the morphological changes of nanoparticles and the response of fluorescence signals was achieved (Figure 8F-M). The in *vitro* release behavior showed that the cumulative release amounts of PTX and cisplatin at 24 h without stimulation were less than 7% and 2.5%, respectively. After adding 1.0 mM H_2O_2, the cumulative release percentage of cisplatin within 12 h was 12%-17%, which was much lower than that of PTX (42%-51%). This might be due to the coordination of cisplatin with Se, which made it difficult to dissociate from the polymer chain. This integrated diagnostic and treatment design enables the precise release of drugs within tumor cells, which minimized harmful side effects in healthy tissues.

In addition to the above types, articles have reported the use of boronate crosslinking groups to prepare ROS-responsive nanomaterials. Wu *et al.* [125] prepared a novel α-TOS dimer through the crosslinking of phenylborate esters. The hybrid nanomedicine 2BOH-TOS/DOX was co-assembled from α-TOS dimers and DOX (Figure 9). Hydrophobic interactions and π-π stacking improve the efficiency of drug loading; additionally, controlled release of the drug can be achieved via the cleavage of boronate esters by H_2O_2. When H_2O_2 was not added, the release rate was significantly restricted, with less than 10% total release within 72 h, demonstrating that it could stably load the drug in a physiological environment and effectively prevent drug leakage or sudden release. The hydrolysis of boronate esters with H_2O_2 is typically a second-order reaction. The rate-determining step is the attack of the boron atom by H_2O_2, which acts as a nucleophile. The rate of this step is directly related to the concentration of both reactants. After H_2O_2 treatment, the release rate of DOX significantly increased. With an increase in H_2O_2 concentration (0.1mM-1.0 mM), the cumulative release amounts reached 52.37% and 69.23%, respectively. The α-TOS component could downregulate intracellular ATP levels, reduce drug efflux, and increase drug concentration, thereby reversing tumor drug resistance.

3.2. Linking drugs to polymers via ROS-responsive bonds to construct polymer nanoprodrugs

To effectively address drug leakage issues in traditional encapsulation systems, drugs can be coupled to the polymer skeleton through ROS-sensitive chemical bonds to construct nanoprodrugs. He *et al.* [126] developed a polyethylene glycol-doxorubicin (mPEG-ROS-DOX) prodrug based on thioketal linkers (Figure 9). This prodrug could be cleaved by ROS in the TME to release DOX. Experiments demonstrated that the prodrug significantly enhanced the drug's half-life and tumor accumulation efficiency in mice with HepG2 tumors by triggering apoptosis in tumor cells, suppressing proliferation, and facilitating necrosis of the tumor cells. Simultaneously, it significantly reduced systemic toxicity and achieved an efficient antitumor effect.

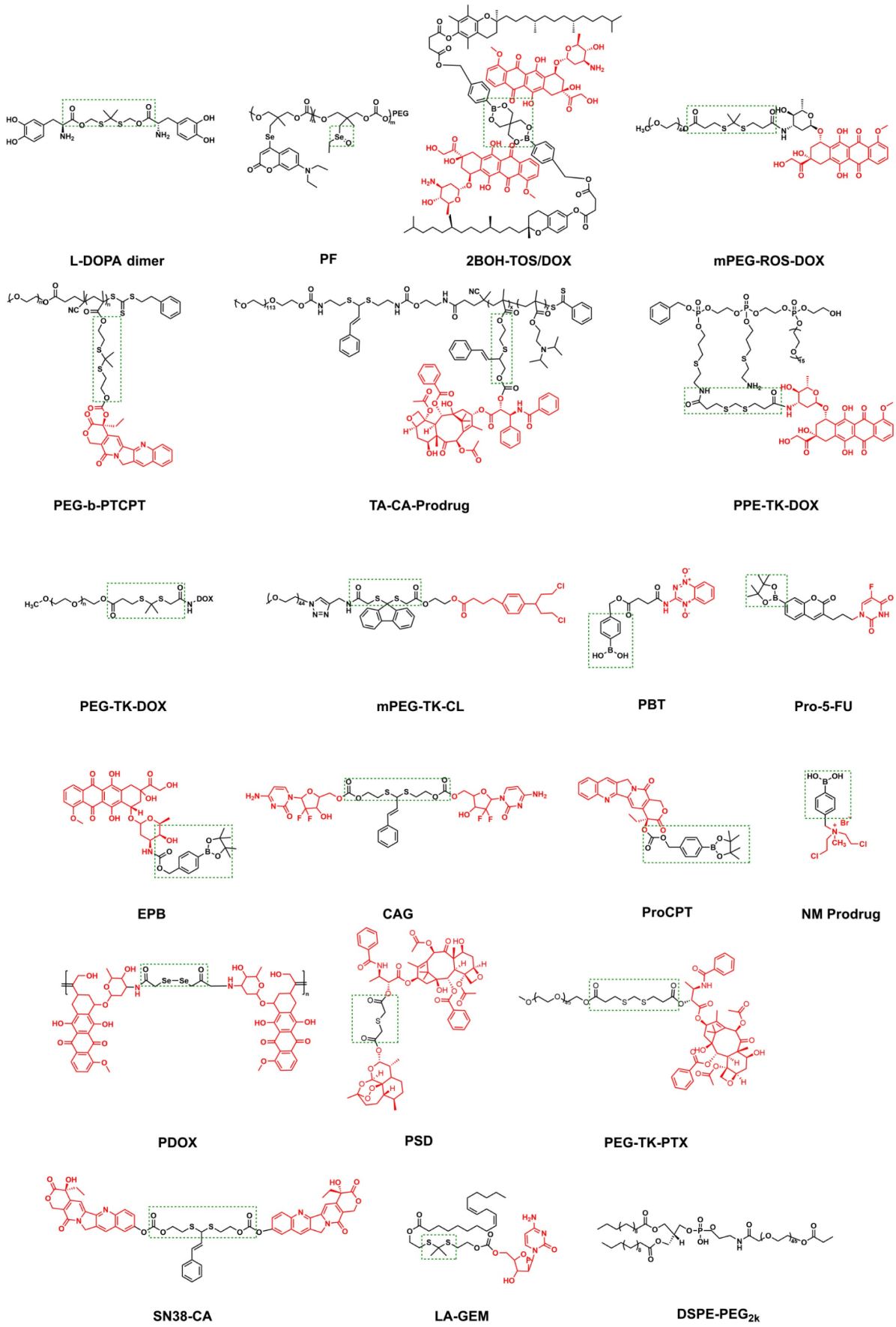

Figure 9. The structure of polymeric nanoprodrugs, the chemotherapy drug (highlighted in red) with a ROS-reactive group (in the green box).

Researchers primarily adopt the strategy of constructing positive feedback ROS-responsive systems to achieve continuous prodrug release post-activation by ROS in cancer cells, thereby realizing the stepwise amplification effect by integrating redox-active molecules or introducing light-responsive dyes or photosensitizers [127]. For example, β-Lapa, an NAD(P)H: NQO1-activating drug, exerts a dual effect by inducing tumor DNA damage and increasing ROS levels in tumor tissues [128]. Ge *et al.* [129] created a novel delivery system utilizing this approach. Initially, they obtained an amphiphilic block copolymer prodrug consisting of PEG and polymethacrylate monomers; then, camptothecin (CPT) was coupled with a thioketal linker and self-assembled into core-shell micelles, PEG-b-PTCPT (Figure 9). Finally, Lapa was encapsulated to construct the composite nanoparticles (Lapa@NPs), which gathered at the tumor in *vivo* experiments. Simultaneously, Lapa selectively elevated the expression of NQO1 in the malignant cells, resulting in the generation of massive amounts of ROS. Elevated ROS levels triggered the rupture of the thioketal linker, thereby releasing CPT and forming a virtuous cycle of "ROS generation-drug release." The released CPT acts in concert with the continuously elevated ROS, significantly inhibiting tumor growth through dual mechanisms: inhibition of topoisomerase I and induction of oxidative stress.

The TA-CA-Prodrug (Figure 9) developed by Luo *et al.* [130] used cinnamaldehyde (CA) as a ROS-responsive thioneone linker to achieve precise coupling of PTX to the copolymer's backbone. A pH-sensitive group, dipropylamine (DPA, pKa≤6.2), was introduced. This prodrug formed micelles through self-assembly, exhibiting a particle size of about 150 nm and a negative ζ-potential. In the acidic conditions prevalent in tumor cells, the protonation of DPA triggered charge inversion (from negative to positive), allowing it to target the negatively charged mitochondrial membrane through electrostatic interactions. The synergistic effect of CA-mediated ROS generation and mitochondrial localization significantly enhanced the specificity and efficiency of drug release. Based on this, Yuan *et al*. [131] performed functional expansion. They coupled the CA linker with DOX and the polymer skeleton, co-loaded the fluorescent prodrug $BCyNH_2$, and self-assembled to form the polyprodrug PEG-TA-CA-DOX, which could be degraded by ROS. Upon entry into the cancer cells, the prodrug was activated by endogenous ROS, resulting in the liberation of a small quantity of bioactive drug. The released CA and $CyNH_2$ induced ROS production through mitochondrial dysfunction, consequently hastening the collapse of PTCD@B and triggering prodrug release.

Spatiotemporally controllable release systems mediated by photosensitizers have become a research hotspot in recent years. Park *et al.* [132] constructed a hydrophilic PEG-DOX conjugate (PEG-TK-DOX) by linking DOX and PEG through thioketal bonds (Figure 9). PEG-DOX could self-assemble into nanoparticle systems with biological activity and ROS responsiveness. DOX release was triggered by ROS generated by the photosensitizer PhA, achieving chemotherapy-photodynamic synergistic therapy. Wang *et al.* [133] co-assembled PPE-TK-DOX (Figure 9) with Chlorin e6 (Ce6) to form nanoparticles (Ce6@PPE-TK-DOX), and utilized the photosensitivity of Ce6 to enhance ROS generation efficiency. Fluorescence imaging conducted in *vivo* revealed that the fluorescence signal was widely distributed throughout the mouse body within 1 h post-injection. Thereafter, the strength of the fluorescence signal from Ce6 at the tumor location gradually rose and peaked at 4 h post-injection. Wang *et al.* [134] also fabricated nanomaterial PSPC NAs using this design concept. Under near-infrared (NIR) light irradiation, photosensitizers generated ROS that spontaneously degraded thioketal bonds and released the drug. Fan *et al.* [135] developed the H_2O_2-activated self-expanding photodynamic/chemotherapy combination therapy drug DPPa NPs. Hydrophobic oxidized bovine serum albumin (BSA-SOH) conjugated with DPPa NPs encapsulated mPEG-TK-CL, an amphiphilic prodrug activated by H_2O_2, along with chlorambucil (CL). (Figure 9). DPPa NPs achieved fluorescence signal recovery and photodynamic effect amplification through BSA-SO_3H coupling, and their macromolecular structure significantly prolonged the tumor residence time (Figure 10). This study provided a reference strategy for prolonging the PDT window period. To address the key challenge of poor permeability of tumor nanomedicines, Bai *et al.* [136] developed a nanomedicine by natural mussel adhesion protein (NMPs), which was conjugated with tilapazine (TPZ) and 4-(hydroxymethyl) phenylboric acid succinic anhydride to form a phenylboric acid prodrug (Figure 9 PBT). After mixing PBT with NMP and doping it with ICG, they obtained ICG-PBT@NMPs nanomedicine. In the TME, the positive charge characteristics were reversed, promoting tumor penetration. Subsequently, tumor cells internalized ICG-PBT@NMPs via endocytosis mediated by arginine transporters. Under near-infrared irradiation, the ICG-PBT@NMPs generated ROS, exacerbating tumor hypoxia and enhancing PBT activation. The design concept based on NMP in this

study could be extended to the design of other drugs.

Noninvasive sonodynamic therapy (SDT) activates sonosensitizers accumulated at tumor sites using ultrasound and stimulates the production of large amounts of ROS. Its tissue penetration ability is stronger than that of PDT. Wan *et al.* [137] constructed a ROS-triggered self-assembled nanoparticle (RP-NPs). RP-NPs were composed of the prodrug LA-GEM (Figure 9) (gemcitabine prodrug with thioketal linker), the natural sonosensitization agent rhein (Rh) (Figure 6), and DSPE-PEG$_{2k}$ (Figure 9). During ultrasound (US) irradiation, Rh was activated and generated a large amount of ROS via acoustic cavitation (Figure 11A). On the one hand, it directly induced apoptosis in the tumor cells. Conversely, it triggered the cleavage of the thioketone bond of LA-GEM, resulting in the targeted and accelerated release of GEM within the tumor (Figure 11B-G). The US could increase the permeability of tumor tissues, improve the hypoxic microenvironment, and synergistically enhance the effect of chemotherapy. SDT could control the treatment range by adjusting ultrasound parameters (e.g., frequency and intensity) and has fewer local side effects (e.g., skin damage). Its biocompatibility is superior to that of PDT and radiotherapy.

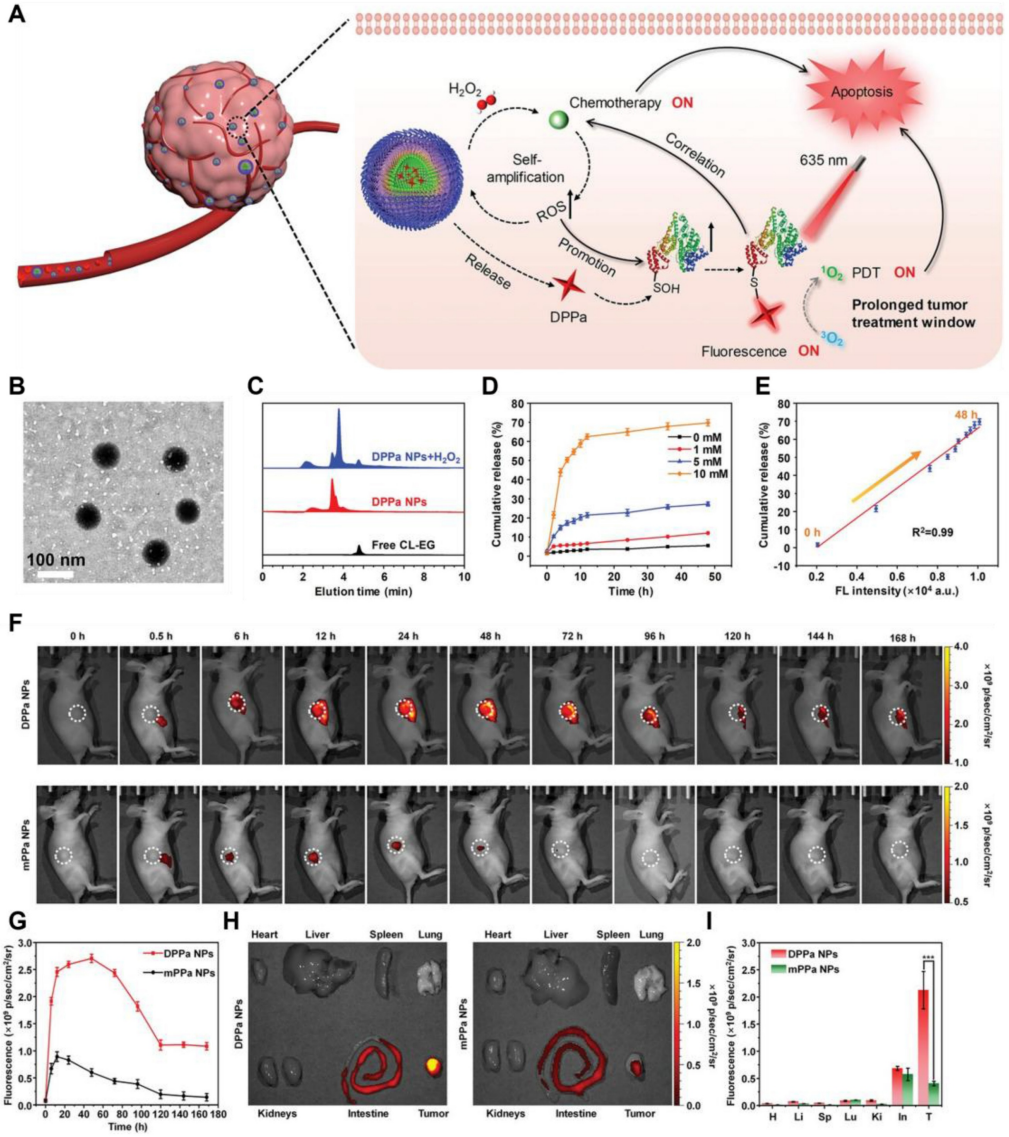

Figure 10. (A) Schematic illustration of fluorescence imaging-guided combined chemo/photodynamic therapy using DPPa NPs to enhance the therapeutic window. (B) TEM image depicting DPPa NPs. (C) HPLC analysis of DPPa NPs (10 μm) following a 1-hour incubation with 1 mM H_2O_2 at 37° C for 1 hour. (D) In *vitro* release characteristics of CL-EG of 1 mM DPPa NPs in PBS at 37°C (pH = 7.4) under different concentrations of H_2O_2. (E) A linear relationship between the fluorescence intensity of DPPa NPs and the release rate of CL-EG. Error bars indicate the standard deviations from three separate measurements. (F) Temporal fluorescence imagery of tumor-bearing mice post-intravenous administration of either DPPa NPs or mPPa NPs (100 μL, 500 μg/mL) (λex = 640 nm, λem =710 nm), with the tumor location indicated by a white circle. (G) Changes in fluorescence intensity within the tumor over time following the injection. (H) Representative images of the major organs and tumors (T = tumor, H = heart, Li = liver, Sp = spleen, Lu = lung, Ki = kidney, In = intestine) of mice 7 days after intravenous injection of DPPa NPs or mPPa NPs. (I) Near-infrared fluorescence intensity. The error bar represents the standard deviations of three different measurements (n = 3), with ***p < 0.001. Reproduced with permission [135]. Copyright 2023, Wiley - VCH GmbH.

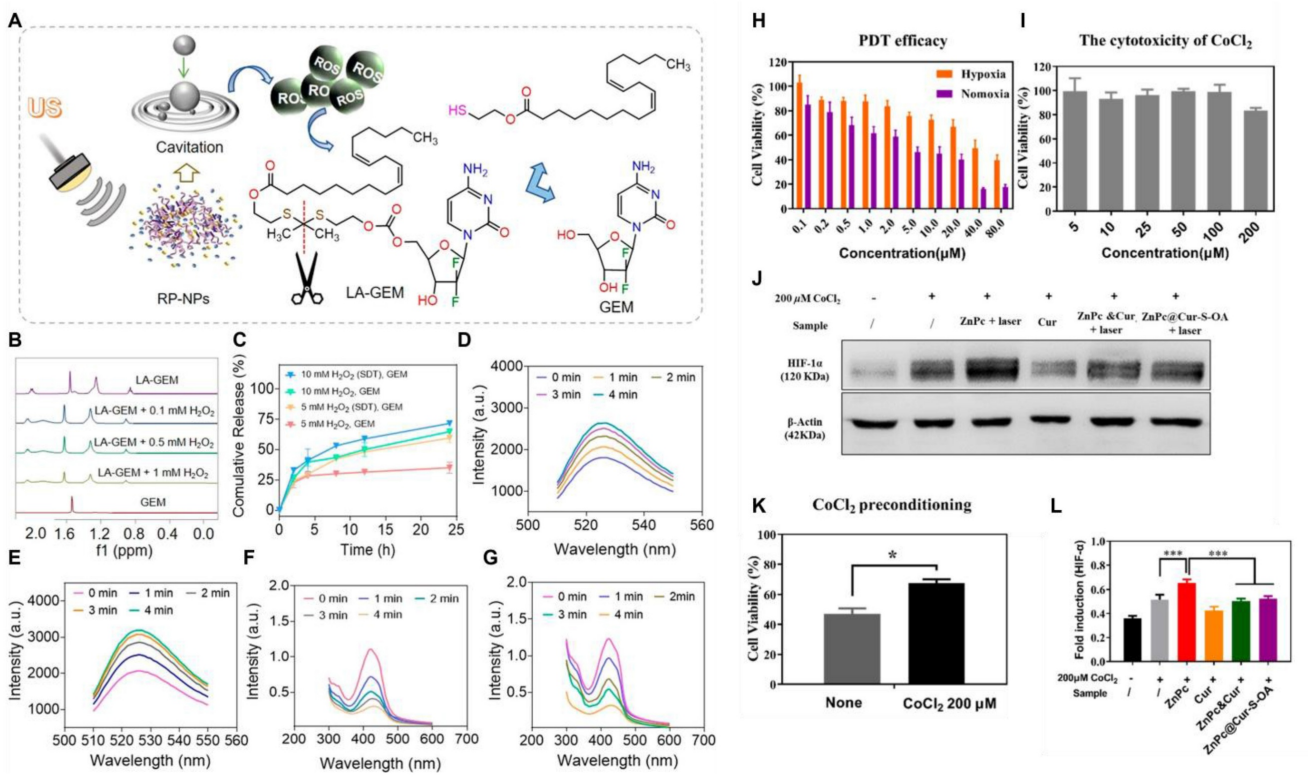

Figure 11. (A) Schematic diagram of GEM release after thione bond cleavage induced by US irradiation. (B) ^{1}H NMR spectra of LA-GEM solution treated with different concentrations of H_2O_2. (C) Release curves of GEM under irradiation with different concentrations of H_2O_2 or US (n = 3). (D, E) Fluorescence intensities of SOSG solution (5 μM) after incubation without (D) or with (E) RP-NPs and then prolonged US irradiation. (F, G) Ultraviolet-visible spectra of DPBF solution (0.1 mg/mL) after incubation without (F) or with (G) RP-NPs followed by prolonged US irradiation. Reproduced with permission [137]. Copyright 2023, American Chemical Society. (H) Cell viability of B16F10 cells after PDT treatment with different concentrations of ZnPc under normoxic or hypoxic conditions. (I) Cytotoxicity of different concentrations of $CoCl_2$ against B16F10. (K) After incubating B16F10 cells with 200 μM $CoCl_2$ for 24 hours, PDT treatment with 10 μM ZnPc was performed to determine the cell viability (N = 12). (J, L) HIF-1α protein levels were determined by Western blot. (N = 3). *, P < 0.05; ***, P < 0.001. Reproduced with permission [138]. Copyright 2020, American Chemical Society.

All the aforementioned self-amplifying nanomedicine systems initiate a cascade reaction by generating ROS via photosensitizers or drugs. The downregulation of GSH disrupts the antioxidant defense system of tumor cells. When ROS activates the prodrug, tumor cells become more vulnerable to drug-induced attacks, thereby overcoming drug resistance [139]. Curcumin (Cur), a natural medicinal component isolated from turmeric, can significantly reduce Hypoxia-Inducible Factor 1α (HIF-1α) levels and consume GSH in various tumor cells [140]. Qu *et al.*[138] designed and fabricated multifunctional combination therapy nanoparticles ZnPc@Cur-S-OA with both self-delivery and self-monitoring capabilities, using Cur as a chemotherapy drug and ZnPc as a photosensitizer. The ROS-activated Cur prodrug (Cur-S-OA) achieved PDT-enhanced cancer treatment by decreasing HIF-1α (Figure 11H-L). The "OFF-ON" activation presented by the green fluorescence of Cur during this process was utilized to monitor drug release.

3.3. Stimuli-responsive materials encapsulate ROS-responsive small molecule prodrugs to construct polymer nanoprodrugs

The polymer nanoprodrugs mentioned above can only respond to a single stimulus, ROS. However, adapting a single response mechanism to the diverse and dynamic changes in the TME is challenging [141]. The pH values, enzyme activities, redox states, and other aspects of the TME between different genres of tumors and the same tumor in different stages of development may be discrepant. It is difficult for drugs with a single response mechanism to cope with these changes, leading to suboptimal specific enrichment and release effects of these prodrugs in tumor tissues, ultimately affecting their therapeutic efficacy [142]. Many recent studies have utilized polymer nanomaterials that can be decomposed under tumor-specific triggering factors (e.g., GSH, pH, and enzymes) as carriers to encapsulate small-molecule prodrugs that can be activated by ROS, thereby constructing dual-responsive DDS [143]. After the outer layer of nanomaterials is disrupted in

the tumor tissue, the encapsulated small-molecule prodrugs are released. These small-molecule prodrugs are further activated by ROS, releasing the chemotherapeutic drugs. The release time and rate of drugs can be more accurately controlled by the dual-response mechanism, thereby better meeting the precise requirements for drug release in tumor therapy.

The high GSH levels in tumor cells can serve as a specific trigger signal in conjunction with ROS. GSH consumption weakens the antioxidant defense of tumor cells, rendering them more susceptible to ROS. In contrast, ROS generation further consumes GSH. These two processes promoted each other, synergistically inducing tumor cell death more effectively and enhancing the antitumor effect of the prodrugs. Zhang *et al.* [144] developed novel cross-linked lipoic acid nanocapsules (cLANCs) connected by disulfide bonds using (R)-(+)-lipoic acid (LA) as the raw material. Both LA and its reduced state (lipoic acid hydride, DHLA) could act as pro-oxidants to increase the generation of ROS within cells. Due to their structural autoploidy with LA, the cross-linked lipoic acid nanoparticles exhibited good biocompatibility and could serve not only as drug carriers but also as pro-oxidants to elevate ROS levels. The ROS-sensitive prodrug, Pro-5-FU (Figure 9), was loaded into H_2O_2-amplifying cLANC to develop the nanoprodrug Pro-5-FU@cLANCs. After entering the cancer cells, they were destroyed by GSH, and LA was released. This process increased the H_2O_2 levels in nanomedicine-treated tumor cells to 3.4 times higher than those in untreated tumor cells, thereby accelerating the release and activation of the prodrug, Pro-5-FU. Gan *et al.* [145] co-delivered the ROS-activated prodrug EPB (Figure 9) and the highly efficient NQO1 substrate KP372-1 by adhesive nanocarriers responsive to GSH. KP372-1 was more effective than existing NQO1 substrates, and a little KP372-1 in NPs exerted a powerful effect on ROS generation but did not exhibit cytotoxic effects. The dual activation of these nanoparticles significantly broadened the selection window between normal and tumor cells.

The low pH of the TME is also widely used as a trigger for the development of nanoparticles. Yang *et al*. [146] constructed pH-responsive micelles through self-assembly using pH-responsive block polymers PEG-Hyd-PCL and cationic block polymers PEI-PCL. Subsequently, these micelles were used to coat the ROS generator β-Lap and the DOX prodrug, BDOX, to form PHI@B/L. The acidic environment in the tumor triggered the cleavage of hydrazone bonds, resulting in the exposure of the positively charged layer and increased uptake of the drug by tumor cells. After the nanosystem was internalized, Lap and BDOX quickly escaped from lysosomes. β-Lap could mediate the generation of ROS, thereby activating the prodrug BDOX and promoting its activation. Furthermore, β-Lap simultaneously consumed ATP, thereby reducing the energy supply of the drug efflux pump and promoting the reversal of multidrug resistance (MDR). This study provided a new perspective for studying the molecular mechanisms in cancer therapy.

Zhao *et al.* [147] synthesized a ROS-activated self-destructing prodrug CAG (Figure 9) using CA and the chemotherapy drug GEM as raw materials. With the help of G ≡ C-type hydrogen bonding interactions, CAG could efficiently bind to the guanine-rich acyclovir-modified hyaluronic acid conjugate HA-ACV and form the supramolecular nanoprodrug HCAG through self-assembly. After injection, the HCAG accumulated at the target tumor site. Subsequently, the acidic environment in the lysosome disrupted the hydrogen bonds, similar to base pairing (G ≡ C) inside the HCAG, causing the structure to disintegrate and the rapid release of free CAG. ROS in tumor cells first activated a small amount of CAG, releasing CA and GEM. CA promoted the production of ROS, which in turn activated the remaining CAG, thereby establishing a self-reinforcing positive feedback loop. Therefore, the HCAG nanoformulation effectively targeted tumors and improved the biodistribution and accumulation of CAG in tumors. Ge *et al.* [148] synthesized the copolymer CAMA-co-ImOAMA using the unstable acetal bond and CA, which was then self-assembled into pH-responsive polymer micelles, and the ROS-responsive prodrug pinacol phenylboronate caged CPT was loaded (Figure 9 ProCPT). The PIMOAMA fragment within the micelles provided nanoparticles with enhanced endosomal escape ability. When micelles ruptured in the tumor cell endosome owing to the acidic environment, the PIMOAMA fragment could breach the endosomal membrane, allowing the released free CA and ProCPT to enter the cytoplasm. CA might increase intracellular ROS levels, thereby enhancing ProCPT activation efficiency. The methylquinone produced during prodrug activation reduced intracellular GSH levels and exerted a synergistic antitumor effect. Zhao *et al.* [149] acetalized maltose (MH) to obtain the pH-sensitized hydrophobic fragment AcMH. Subsequently, a click reaction linked the hydrophilic segments PAsp and mPEG to form amphiphilic block polymers PAsp-AcMH and mPEG-AcMH. mPEG-AcMH and PAsp-AcMH self-aggregated with the nitrogen mustard (NM) prodrug (Figure 9) and

Lapa to form nanoparticles. Following intravenous injection, these nanoparticles could localize at the tumor site. The weakly acidic environment caused the acetal bond to break and released the NM prodrug and Lapa. Lapa induced the production of a large amount of H_2O_2, which further activated NM prodrug. The control of precise drug release by dual-responsive nanoprodrugs was primarily reflected in the "silencing" of non-target environments, the "specific activation" of target environments, and the "synergistic filtering" effect of dual signals. Liu *et al.* [150] linked DOX to the polymer main chain *via* an acid-labile hydrazone bond and a diselenide (Figure 9 PDOX). The release of DOX required simultaneous satisfaction of two conditions: low pH and a high level of ROS. In a medium with a pH of 7.4, even at a GSH concentration of 10 mM (far exceeding the level in normal tissues), drug release was negligible. Meanwhile, at pH 5.0 of tumor areas, but with a GSH concentration of zero or low level (0.1 mM, non-tumor feature), the drug is also hardly released. The drug showed detectable cumulative release (10.3% and 7.4% within 96 h) only at pH 5.0 (acidic) and in the presence of high concentrations of GSH (10 mM) or H_2O_2 (0.5 mM). The "dual filtering barrier" not only avoided the accidental leakage of drug molecules in nanomedicines designed through only one controllable condition but also significantly improved the drug-loading capacity of nanocarriers.

3.4. Iron-coordinated nanocarriers encapsulating small molecule prodrugs to construct polymer nanoprodrugs

Fe^{2+} and Fe^{3+} can generate ROS by Fenton or Fenton-like reactions [151]. Fe^{2+} can also reduce H_2O_2 to OH•, thereby causing cell damage [152]. Tumor cells highly express the transferrin receptor (TfR1), which absorbs more iron to meet their rapid proliferation requirements. Introducing iron into prodrugs exploits the high iron uptake characteristics of tumor cells, enabling prodrugs to enter tumor cells more effectively through TfR1-mediated endocytosis [153]. Therefore, previous studies have utilized iron-coordinated nanocarriers to deliver small-molecule prodrugs activated by ROS. Chemotherapeutic drugs often used in combination with iron-coordinated nanocarriers include PTX and dihydroartemisinin (DHA). Research indicates that inducing ferroptosis in cancer cells can overcome their resistance to paclitaxel therapy. For instance, innovative taxane SB-T-101141 initiated ferroptosis through an iron-stable-related mechanism involving KHSRP, thereby overcoming paclitaxel resistance in breast cancer (Figure 12A-H) [154].

Yin *et al.* [156] linked PTX and DHA through a thioether bond to synthesize a prodrug that could be activated by ROS (Figure 9). This prodrug self-assembled to form PTX-S-DHA nanoparticles, which exhibited a significant capacity for drug loading. While tumor cells exhibited a greater concentration of H_2O_2 compared to normal cells, it was easily consumed, thereby limiting the number of OH• produced by the Fenton reaction. Therefore, the self-assembly prodrug PSD was co-precipitated with PEG2000-ferrous iron (Fc) to create nanoparticles known as PSD-Fc nanoparticles. In the presence of Fe^{2+}, DHA exhibited catalytic activity resembling that of a peroxidase, which promoted the Fenton reaction within cells, resulting in the production of a significant quantity of ROS. The synergistic effect of PTX led to the death of tumor cells. To achieve effective co-transport of iron toxicity inducers, exogenous ferrous ions, and chemotherapeutic drugs. Similarly, Zhang *et al.* [155] coupled PTX with ferrocene (Fc) using thiophenone to prepare the DHA-loaded nanocells ($^{TK}NP_{DHA}$-Fc) (Figure 9 PEG-TK-PTX). Through the synergistic effects of chemotherapy and ferroptosis, significant antitumor effects were demonstrated both in *vivo* and in *vitro* (Figure 12I-J). Kamei *et al.* [157] prepared nanoparticles SN38-CA@FC NPs (Figure 9 SN38-CA) using a one-step nano-precipitation method. They linked the CPT derivative SN38 to the ROS generator CA via thioacetone and co-assembled it with Fc. SN38-CA@FC nanoparticles induced the accumulation of lipid peroxides (LPOs) by consuming GSH and GPX4, ultimately triggering severe oxidative damage and cell death. This intelligent precursor nanosystem, composed of ferroptosis inducers and chemotherapy drugs, maximized the effects of ferroptosis and chemotherapy by leveraging the Fenton reaction.

4. ROS-Triggered Hydrogel Prodrugs

As a hydrophilic substance, hydrogels have become an essential supplement to nanoparticle DDS because of their safety to normal tissues [158]. Compared to nanoparticle carriers, hydrogels offer unique advantages in drug delivery, particularly with broad application prospects in cancer treatment. Over the past few years, hydrogel DDS have evolved from passive release to intelligent controlled-release systems that can react to diverse external stimuli, including pH, ROS, heat, light, and ultrasound, and have further developed in the direction of multi-responsive collaborative regulation [159]. Among them, ROS-responsive hydrogels can achieve targeted drug release by introducing specific reaction units that cause hydrophilic and hydrophobic transitions of polymer chains or break chemical bonds

in a high ROS environment [12,160]. This section focuses on discussing this type of drug delivery hydrogel systems responsive to ROS through solubility conversion or bond cleavage mechanisms (Figure 13).

4.1. Hydrogels with solubility switch units

Miryam *et al.* [161] have developed a novel water-soluble redox-responsive monomer based on ethylene glycol thioacrylate (EG_nSA), which could be polymerized by ultraviolet light (UV) and form a 4D printable hydrogel exhibiting high-resolution properties. The antitumor drug 5-fluorouracil (5FU) was encapsulated in the hydrogel system. Notably, the sulfide groups in the EG_nSA molecule changed to hydrophilic sulfoxide or sulfone groups under the action of H_2O_2 or hypochlorite, thereby triggering the expansion of the hydrogel network and facilitating controllable drug release (Figure 14A-D).

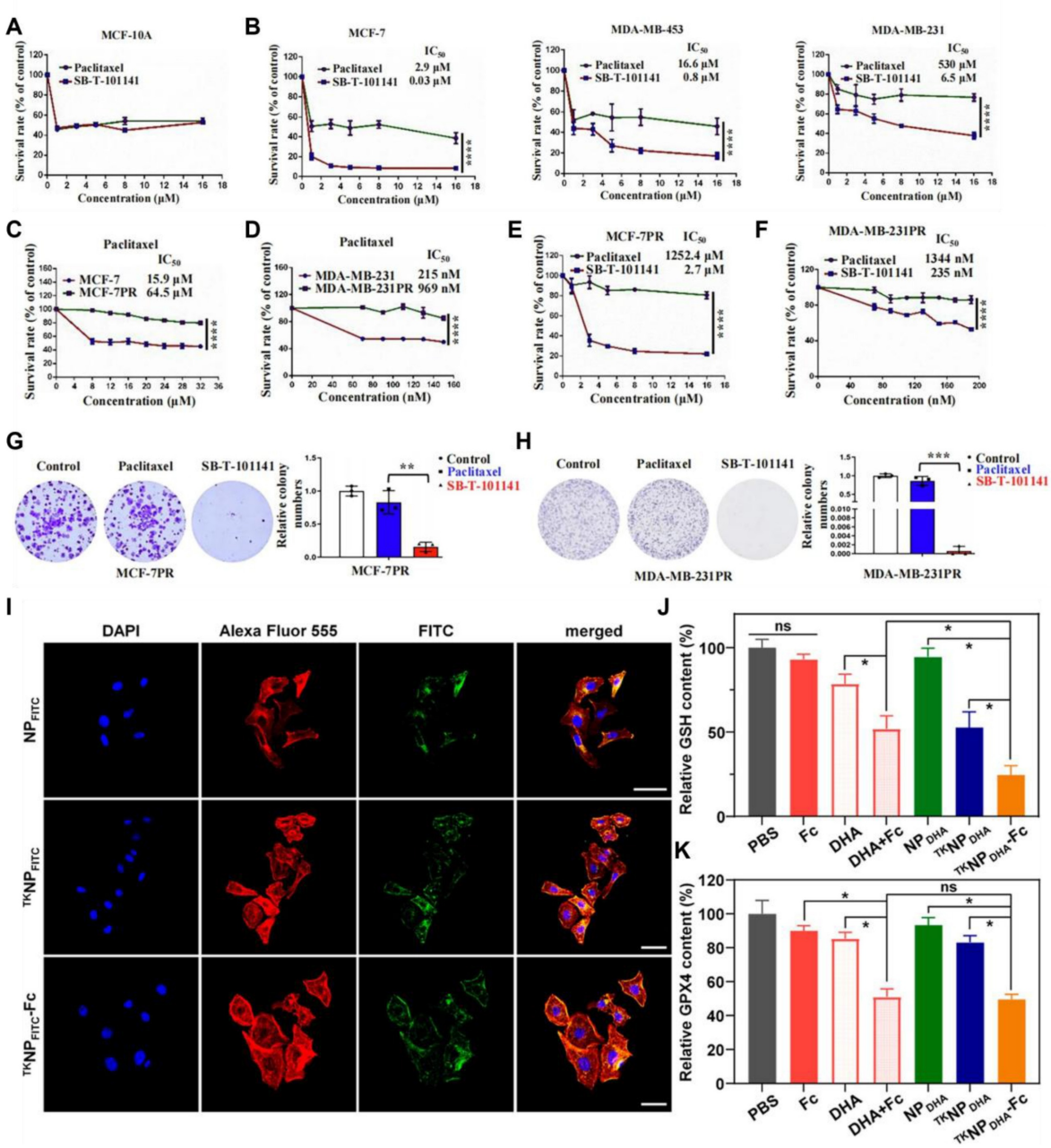

Figure 12. (A, B) Cell viability analysis of different cell lines after 72 hours of treatment with paclitaxel and SB-T-101141 at specified concentrations. (C-F) Viability analysis of drug-resistant cells (MCF-7PR, MDA-MB-231PR) and non-drug-resistant cells (MCF-7, MDA-MB-231) 72 hours after administration. Results were analyzed using a Two-way *ANOVA* test (mean ± SD, n = 3). *P < 0.05, **P < 0.01, ***P < 0.001, and ****P < 0.0001. (G, H) Crystal violet staining after MCF-7PR and MDA-MB-231PR cells were treated with paclitaxel or SB-T-101141. Results were analyzed using a Student's t-test (mean ± SD, n = 3) (right panel). *P < 0.05, **P < 0.01, ***P < 0.001, ****P < 0.0001. Reproduced with permission [154]. Copyright 2025, Springer Nature. (I) CLSM observation of 4T1 cells treated with FITC-loaded NP, ^{TK}NP, or ^{TK}NP-Fc. The scale bar is 50 μm. (J, K) Relative glutathione level and content of GPX4 in 4T1 cells upon incubation with different formulations (mean ± SD). Fc equivalent concentration was 10 μM. ns, no significant differences. *p < 0.05. Reproduced with permission [155]. Copyright 2024, American Chemical Society.

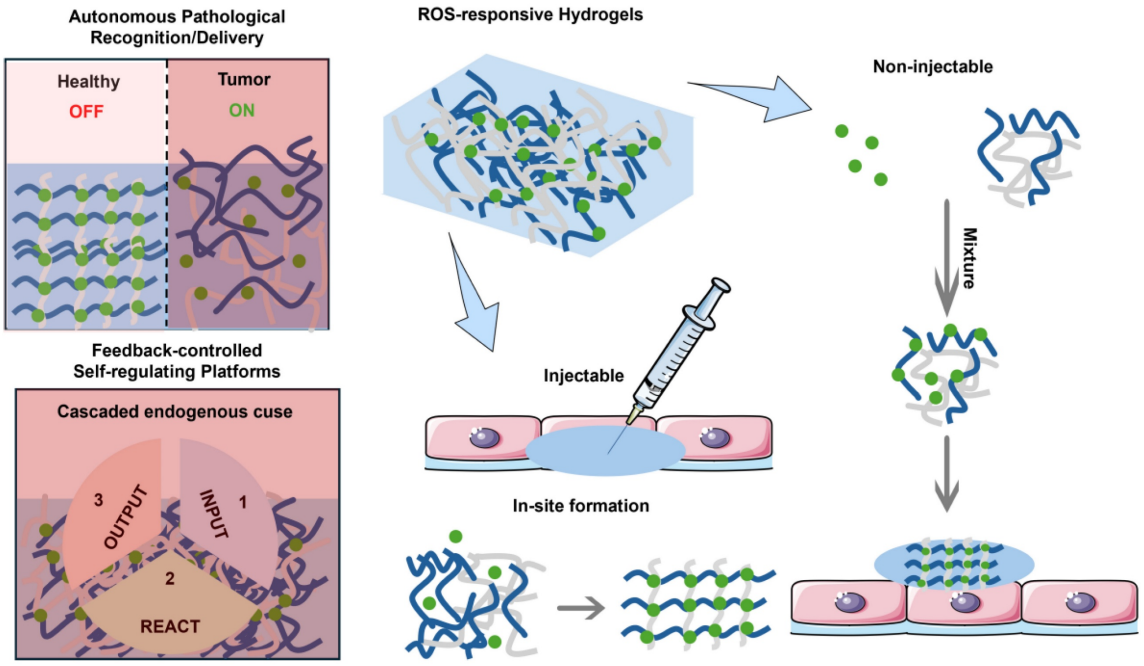

Figure 13. The drug release mechanism of hydrogels triggered by ROS: Two types of ROS-responsive hydrogels (injectable and non-injectable) have achieved site-specific drug release by taking advantage of the ROS in the TME, and have the benefits of local retention, controllable release, and multimodal treatment.

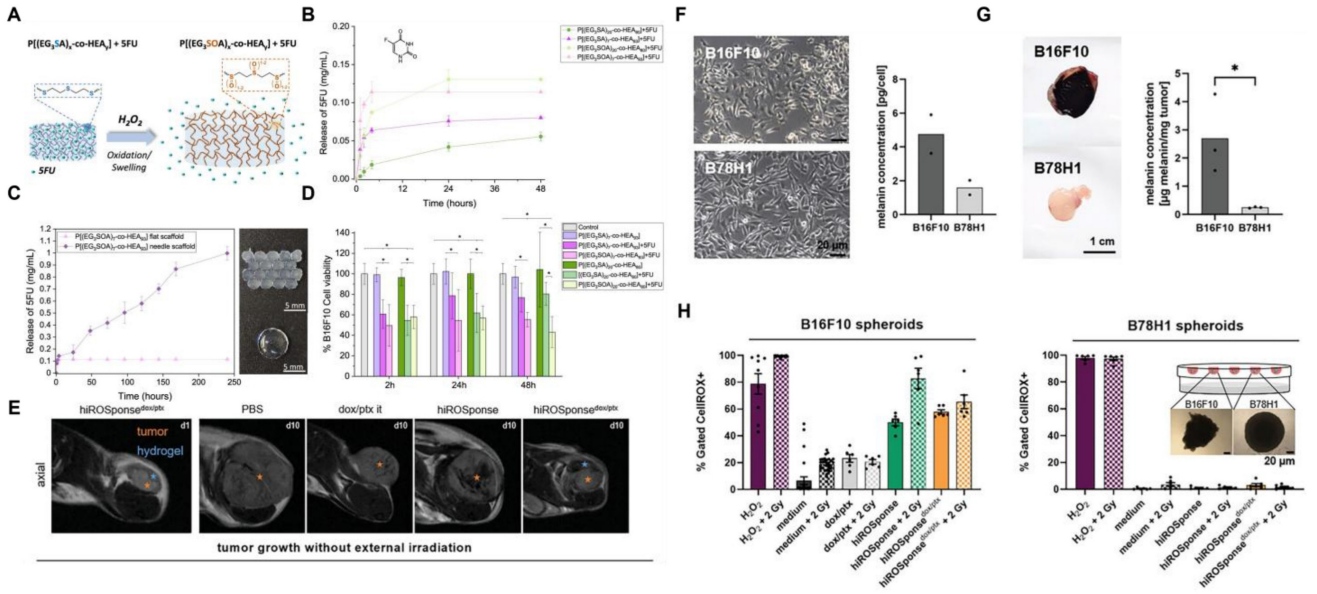

Figure 14. (A) Schematic depiction of the release of 5FU from P[$(EG_nSA)_x$-co-HEA_y] hydrogels, which is facilitated by oxidation and swelling in a system that contains H_2O_2. (B) Release of 5FU from hydrogels (P[$(EG_3SA)_{20}$-co-HEA_{80}] and P[$(EG_3SA)_7$-co-HEA_{93}]) was examined under non-oxidative conditions in PBS as well as under oxidative conditions with the inclusion of 9 mM H_2O_2. (C) The two types of P[$(EG_3SOA)_7$-co-HEA_{93}] hydrogels (needle scaffold and flat surface scaffold) release 5FU when subjected to oxidizing conditions (1 mM H_2O_2). (D) Evaluation of P[$(EG_3SA)_{20}$-co-HEA_{80}] and P [$(EG_3SA)_7$-co-HEA_{93}] release of 5FU of B16F10 in vitro cytotoxicity. One group was under non-oxidizing conditions, where cells were co-cultured with hydrogels in PBS. Another group was under oxidation conditions, with an additional 1 mM H_2O_2 added to the co-culture system. All experimental data were expressed as "mean ± standard deviation" (sample size n=3), and the Tukey test was used for analysis of variance, with the significance level set at *p < 0.5. Reproduced under terms of the CC BY 4.0 license [161]. Copyright 2023, by Miryam *et al.* (E) Representative magnetic resonance imaging (MRI) of subcutaneous solid B16F10 tumor (orange mark) and the injected hydrogel (highlighted in blue) are shown at day 1 and day 10 post hiROSponse injection. (F) The structure of cells and the amount of melanin in melanotic B16F10 and B78H1 cells when grown in a monolayer culture. (G) Samples of B16F10 and B78H1 tumors were representative, and melanin levels were quantified in the excised tumor specimens. A two-tailed unpaired t-test was utilized for statistical evaluation, with a significance threshold set at *p < 0.05 and a sample size of n=3. (H) Flow cytometry was employed to measure the levels of ROS in spheroids of B16F10 and B78H1. Cells were selected based on the fluorescence signals that were positively emitted by the CellROX probe. The range of sample sizes varied from n=5 to n=29, with all results presented as mean ± standard error. An image is provided depicting the microscopic observation of B16F10 and B78H1 spheroids after a culture period of four days utilizing the hanging drop technique. Reproduced under terms of the CC BY 4.0 license [162]. Copyright 2024, by Hauser *et al.*

Compared with traditional preformed hydrogels, injectable hydrogels can be formed in situ using minimally invasive surgery, effectively covering areas that are hard to reach with traditional surgical approaches. Free chemotherapy drugs that are directly injected into the tumor site can be quickly cleared by the circulatory system. In contrast, hydrogel DDS can maintain a long-lasting local drug concentration in tumors. Based on this, Hauser *et al.* [162] constructed an injectable ROS-responsive hydrogel (hiROSponse) using Fc to co-load the melanoma treatment drugs DOX and PTX. Hydrophilic DOX was physically embedded in the hydrogel network, and its release followed the Fick diffusion mechanism. The hydrophobic drug PTX was loaded via hydrophobic interactions with Fc. In the microenvironment with a high redox potential specific to melanoma, Fe^{2+} was oxidized to Fe^{3+}, resulting in the disruption of hydrophobic interactions, thereby achieving the specific release of PTX. In tumor studies, injection of PBS, dox/ptx, hiROSponse, hiROSponse^{dox}, or hiROSponse^{ptx}, hiROSponse$^{dox/ptx}$ significantly slowed the tumor growth (Figure 14E-H).

Immunotherapy activates the immune system through the use of immunomodulatory drugs, antibodies, or adjuvants. However, the nonspecific biological distribution of immunotherapeutic drugs often leads to insufficient response rates and adverse immune reactions. It is essential to create nano-delivery systems capable of continuously releasing drugs in tumors. Chen *et al*. [163] have developed an innovative ROS-responsive injectable thermogel system. This system was based on a methoxy PEG block polysulfide copolymer (mPEG-b-PMet) co-loaded with the chemotherapy drug DOX, antiviral drug imidazoquinoline, immunomodulator R848, and immune checkpoint inhibitor αPD-1. The gel solution underwent a temperature-responsive sol-gel transformation after being injected into the tumor site. Its methionine methyl sulfide group was oxidized to sulfoxide units by ROS, triggering the regulated release of the drug. In the B16F10 melanoma mouse model, the hydrogel co-loaded with DOX/R848/αPD-1, when locally injected, not only suppressed tumor growth and extended survival but also elicited a robust anti-tumor immune response while maintaining low systemic toxicity. Notably, this system also demonstrated an outstanding ability to prevent recurrence and foster long-term immune memory effects, confirming the clinical translational potential of the hydrogel-based local chemoimmunotherapy strategy.

4.2. Hydrogels with cleavable units

In addition to the solubility transformation mechanism triggered by ROS, studies have reported the integration of fracture units that react with ROS into the hydrogel. This ROS-responsive hydrogel can control drug release by breaking the polymer chain under oxidizing conditions, ensuring that the hydrogel is completely degraded into nontoxic molecules and avoiding long-term retention caused by immune responses.

Hydrogels prepared from natural polymers exhibit remarkable biocompatibility, degradability, and flexibility, making them extensively employed in biomedical applications. Carboxymethyl cellulose (CMC), sourced from natural cellulose, presents outstanding development opportunities. CMC exhibits significant physical and chemical characteristics, including water absorption, film-forming ability, and low immunogenicity, in biological fluids. However, the low mechanical strength and rapid degradation limit their application in biomedicine. Therefore, they must be modified to obtain hydrogels with better mechanical properties and higher drug-loading efficiency. Lim's team [164] constructed a mechanically stable biomedical hydrogel through an inverse electron-demand bond reaction involving Tz and Nb. The nitrogen byproduct promoted the development of a porous structure within the hydrogel. The photosensitizer ICG and chemotherapy drug DOX were coated onto a porous network. Under near-infrared light irradiation, ICG generated ROS, broke the thioketal bond, disrupted the hydrogel structure, and released drugs. Some studies have also utilized ROS to induce the in-situ formation of hydrogels and bioorthogonal reaction-mediated prodrug activation. Gao *et al.* [165] developed a self-reporting system for the activation of bioorthogonal prodrugs. The Tz group serves as both a fluorescence quencher and a prodrug activator. When it underwent Diels-Alder (IEDDA) reaction with the prodrug TCO-PTX, which was modified with trans-cyclooctene (TCO), it relieved the fluorescence quenching. It released the active drug, and the fluorescence intensity is linearly related to the amount of drug released.

Li *et al.* [60] utilized the calcium-induced gel properties of alginate to construct an injectable in-situ formed hydrogel. The alginate solution contained PpIX-modified Fe_3O_4 nanoparticles (PF) and programmed death ligand 1 antibody (αPD-L1), which were linked to BSA using ROS-responsive linkers. The photosensitizer PpIX produced $^1O_2$ under near-infrared light irradiation for photodynamic therapy. Fe_3O_4 could undergo a Fenton reaction to produce OH• and exert chemotherapeutic effects.

Table 4. ROS-triggered hydrogel prodrugs.

Name	Drug	Activable group	*In vitro*/*in vivo* model	Therapeutic effect	Refs
P[(EG_3SA)$_x$-*co*-HEA_y]	5-FU	Thioether	B16F10	The viability of B16F10 cells decreased by approximately 60% at 2 hours and dropped to approximately 80% after 48 hours.	[161]
hiROSponse$^{dox/ptx}$	DOX/PTX	$FeCp_2$	B16F10 melanoma-bearing mice	Compared with local injection of DOX without the use of a hydrogel matrix, this hydrogel could significantly reduce tumor growth by approximately 50%.	[162]
Dox/R848/aPD-1@Gel	DOX/R848/αPD-1	Methylthio group	B16F10 melanoma-bearing mice	The Dox/R848/aPD-1@Gel group demonstrated significantly stronger anti-tumor effects, with an average tumor volume of less than 300 mm^3.	[163]
CMC hydrogels	DOX	Thioketal	HeLa	The cell survival rate of the DOX (20 μg) treatment group was approximately 6.5%, while that of the DOX+ICG encapsulated hydrogel (with equivalent DOX concentration) treated with near-infrared irradiation reached 6.7%.	[164]
TCO-PTX	PTX	-	MCF-7 cell spheroids	The prodrug activation process led to an increase in the number of dead cells within the cell spheres.	[165]
APPF hydrogels	αPD-L1	Thioketal	subcutaneous bilateral 4T1 tumor models	In the APPF + laser group, the average number of pulmonary metastatic nodules was found to be 0.8, indicating a reduction of 2.1 times compared to the APPF treatment group, and 16.7 times less than that observed in the PBS control group.	[60]

Table 5. ROS-triggered inorganic nanoprodrugs.

Name	Drug	Activable group	*In vitro*/*in vivo* model	Achievement	Refs
MSN@TheraVac	*a*PD-L1	Diselenide	Balb/c mice bearing an ectopic CT26 tumor model	After MSN@TheraVac treatment, the tumor-bearing mice initially exhibited slow tumor growth. Still, they then began to experience tumor shrinkage after the third treatment, and complete regression was finally observed after the fifth treatment.	[170]
T/D@RSMSNs	DOX/α-TOS	Thioketal	MCF-7 tumor bearing mice	The group that received injections of T/D@RSMSNs exhibited a notable reduction in tumor growth, and no systemic side effects were observed.	[172]
MTN@DTX-CD	DTX	Thioketal	S180 tumor bearing mice	In the MTN@DTX-CD+US group, the tumor volume decreased by approximately 60% within 15 days.	[171]

The production of large amounts of ROS could lead to immunogenic cell death (ICD) and disrupt thiol bonds, releasing αPD-L1. αPD-L1 bound to PD-L1, blocking tumor immune escape mediated by the PD-1/PD-L1 pathway and enhancing the killing activity of T cells against tumor cells. The hydrogel platform of this prodrug exhibited dual responses to the TME and near-infrared light, which prominently restrained the development of both primary breast cancer tumors and metastatic lesions and effectively prevented metastasis in the lungs and liver. Immunofluorescence staining indicated an elevation in the expression levels of calreticulin (CRT) and high-mobility group protein B1 (HMGB1) within tumor tissues following APPF+laser treatment, thereby promoting dendritic cells (DCs) maturation.

5. ROS-Triggered Inorganic Nanoprodrugs

Inorganic nanoparticles include inorganic particles and biodegradable polycationic synthesis [166]. Materials with mesoporosity exhibit elevated specific surface areas, significant pore volumes, and tunable mesoporous architectures and compositions. They have great potential in environmental protection, energy storage and conversion, biomedicine, and other fields [167]. Among them, mesoporous titanium dioxide nanoparticles (MTNs) and mesoporous silica nanoparticles (MSNs) possess characteristics such as uniform pores, easy functionalization, elevated specific surface area, substantial pore volume, favorable biocompatibility, and biodegradability [168,169]. In particular, MTNs and MSNs induce the generation of ROS in several cell lines, indicating their potential in creating DDS that respond to ROS. Thus, this section discusses such systems based on MTNs and MSNs (Figure 15).

The most common method for developing the DDS using ROS-responsive MSN involves the direct conjugation of drugs to the nanoparticle surfaces via ROS-sensitive linkers. Yang *et al.* [170] developed mesoporous silica nanoparticles (MSN@TheraVac) that responded to ROS for colon cancer therapy. The nanoparticles had αPD-L1 attached to their surface through diselenide bonds, and they incorporated high mobility group nucleosome-binding protein 1 (HMGN1) along with resiquimod/R848. αPD-L was rapidly released under oxidative conditions, thereby avoiding both immune suppression and the exhaustion of effector T cells. Simultaneously, HMGN1 and R848 worked together to enhance the maturation of potent tumor-infiltrating dendritic cells (DCs), which in turn stimulated antitumor immune responses. Free TheraVac could be immediately used for DC stimulation, the TheraVac encapsulated in MSN@TheraVac required prior release. This likely induced delayed DC stimulation, which in turn promoted the secretion of Tumor Necrosis Factor-α (TNF-α) and Interleukin-12/Interleukin-23 (Figure 16A-F). Through intravenous injection therapy,

MSN@TheraVac achieved a 100% cure rate in BALB/c mice with colorectal tumors. Other cancer vaccines can also be delivered using this ROS-responsive MSN platform, thereby achieving selective and effective immunotherapy.

Gated DDS maintain the drugs in a stable encapsulation state under normal physiological conditions through gating groups. In recent years, numerous stimulus-responsive, controllable drug release carrier systems have been developed using inorganic nanoparticles, synthetic polymers, peptides, cyclodextrins, and DNA/RNA as mesoporous "gating switches" for micropores. Zhang *et al.* [172] investigated a nanodelivery system (T/D@RSMSN) for drug release that is self-accelerating and triggered by ROS. The gated β-cyclodextrin (β-CD) group was linked to MSN through ROS-cleavable thioketal. The PEG chain of conjugated adamantane further modified the surface of the carrier through host-guest interactions. The DOX and ROS products, α-TOS, were encapsulated in the carrier. The intensity of fluorescence from DOX in MCF-7 cells showed that, under the action of α-TOS, the release rate of DOX (36 h) increased by 1.9 times. This indicated that the thioketal linker dissociated in the MCF-7 cells, after which DOX and α-TOS were released. The liberated α-TOS additionally elevated the levels of intracellular ROS and promoted the release of DOX. Similar to MSNs, MTNs have an appropriate drug-loading pore size and low cytotoxicity, making them another ideal carrier for stimulating reactive DDS. MTN is capable of producing substantial amounts of ROS by absorbing UV radiation or by focused US treatment. Zhang *et al.* [171] utilized the thioketal linker to connect β-CD to the outer surface of the MTNs as the gating group. This system encapsulated DTX. After two 40-second US treatments, the total release rate of DTX after 24 h was 96.8%. The release rate in the untreated group was only 7.5%. In a mouse model with tumors, focused US at the tumor location enhanced the efficacy of combination therapy and inhibited tumor growth. The tumors in the MTN@DTX-CD+US group decreased in size by approximately 60% within 15 days (Figure 16G-O).

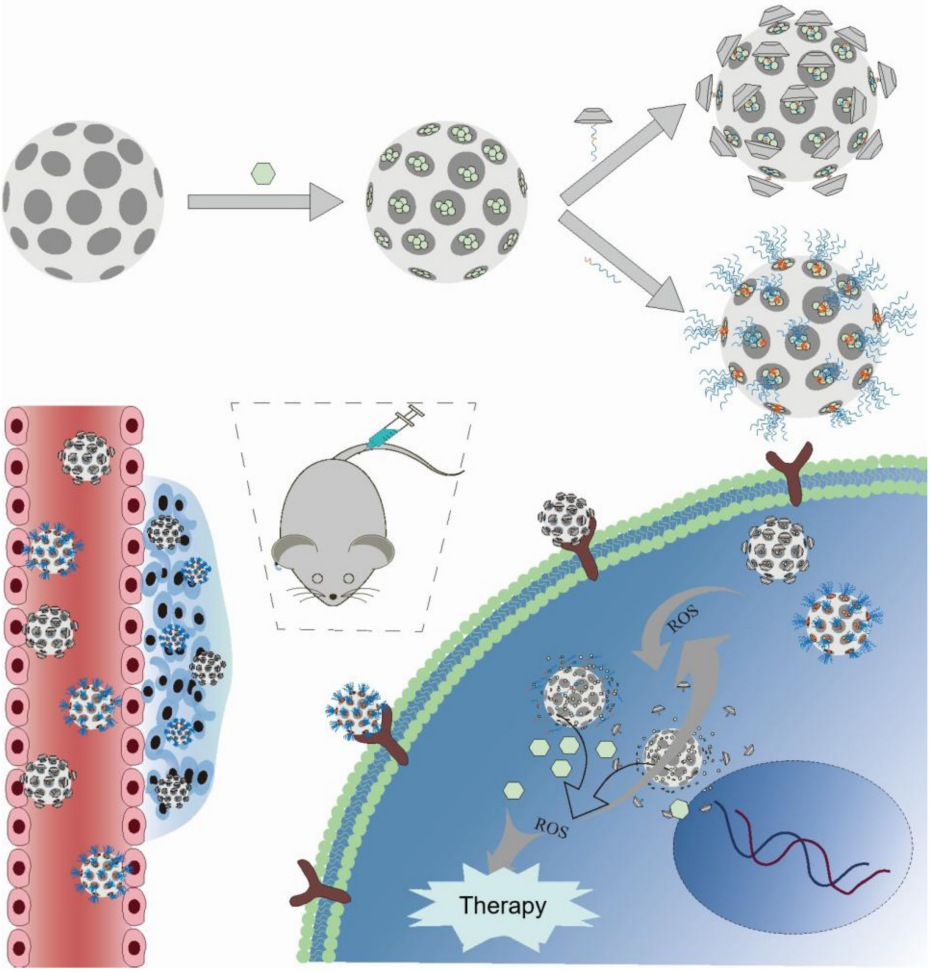

Figure 15. The ROS-triggered drug release mechanism of inorganic nanoparticles in tumor treatment. MSNs and MTNs are key inorganic carriers for ROS-responsive drug delivery. Their surfaces are linked to "gated molecules" through ROS-responsive linkers, preventing premature drug leakage. After functional modification, targeted drug release and imaging localization can be achieved. Meanwhile, tumor-targeting ligands are transplanted onto the surface of nanoparticles to enhance receptor-mediated endocytosis.

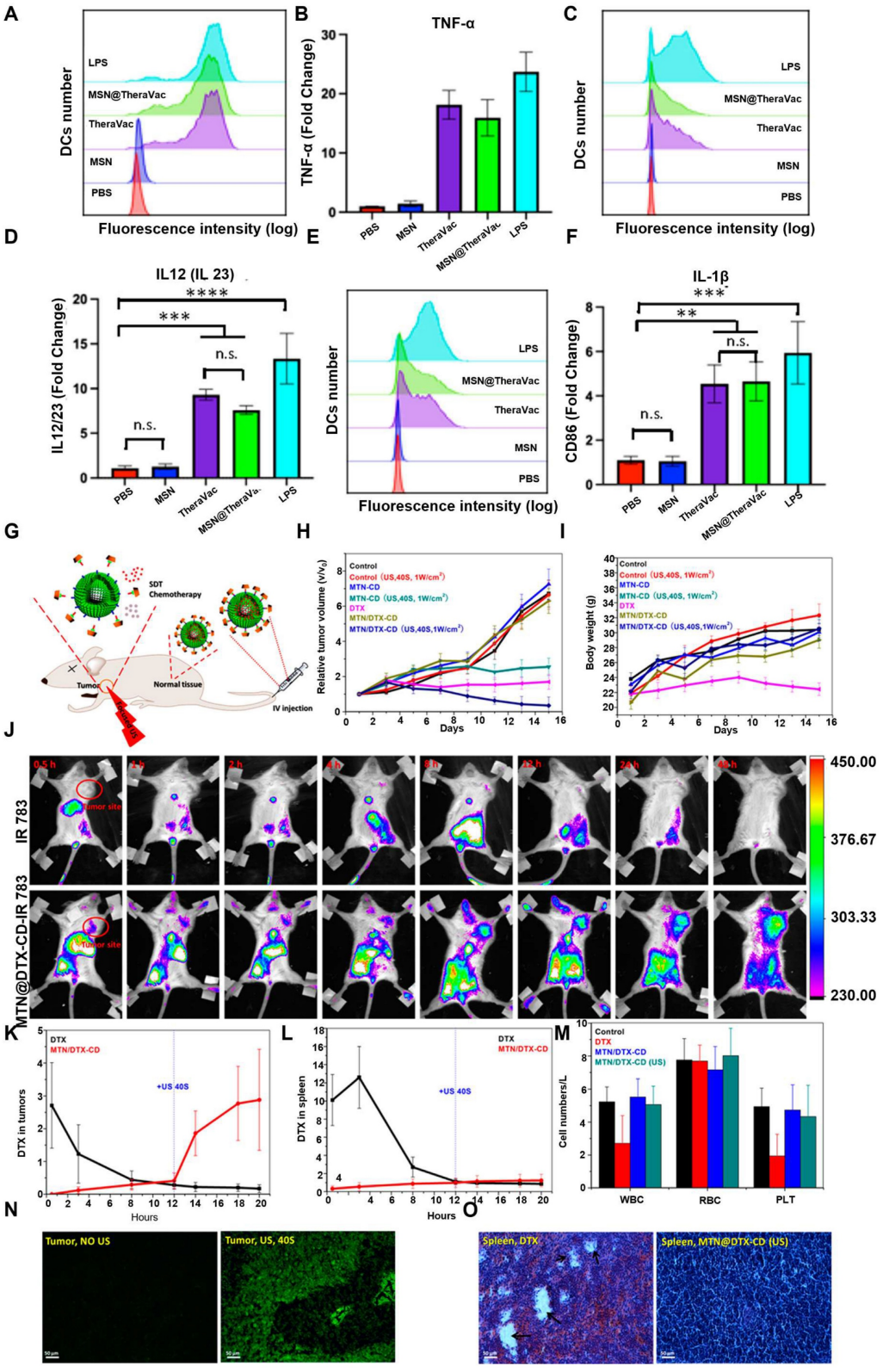

Figure 16. (A-F) Measurement and quantification of TGF-α, IL-12/ IL-23, and IL-1β through flow cytometry analysis of mouse bone marrow-derived DCs treated with unloaded MSN, free TheraVac, MSN@ TheraVac, and LPS. *p < 0.05, **p < 0.01, ***p < 0.001, ****p < 0.0001, n.s. nonsignificant. Reproduced with permission [170]. Copyright 2023, American Chemical Society. (G) Schematic representation of the SDT chemotherapy. (H) Mouse tumor growth in distinct treatment groups during the 15-day observation (n = 6). (I) Mean body weight change of mice after different treatments (n = 6). (J) NIR imaging of tumor-bearing mice at 0.5, 1, 2, 4, 8, 12, 24, and 48 hours after intravenous injection of free IR783 solution and MTN@DTX-CD-IR783. (K) Levels of DTX in tumors 20 hours following injection of DTX and MTN@DTX-CD (n = 3). (L) Spleen-associated DTX levels measured 20 h post-administration of DTX and MTN@DTX-CD (n = 3). (M) WBC, RBC, PLT cell counts in tumor-bearing mice with distinct treatments for 15 d (n = 6). (N) Fluorescence images displaying FITC (green) in tumors following a 12 h injection of MTN@FITC-CD, with and without US radiation. Scale bar: 50 Mm. (O) Images of H&E staining from spleens of mice that received 15 days of treatment with DTX and MTN@DTX-CD (US) are shown. The data are expressed as mean ± standard deviation. Scale bar: 50 μM. Reproduced with permission [171]. Copyright 2015, American Chemical Society.

Table 6. Comparison of different ROS-responsive drug delivery systems.

System type	Core carrier/structure	ROS response mechanism	Targeting ability and delivery efficiency	Degree of functional integration	Safety
Small Molecule Prodrugs	Direct modification of drug molecules.	The drug is released through bond breakage.	Passive targeting (high ROS dependent on tumors), strong tissue penetration, but weak targeting.	The main focus is on drug release.	The structure is clear and the metabolic pathway is distinct.
Polymeric Nanoprodrugs	Polymer skeletons (such as PEG derivatives, polyamino acids).	Bond breakage or hydrophilic and hydrophobic transformation.	Active targeting (modified ligands) + passive targeting (EPR effect), with high tumor accumulation efficiency (3 to 5 times that of free drugs).	It can carry chemotherapy drugs, photosensitizers, etc., to achieve synergistic treatment.	Rely on the biocompatibility of polymers.
Hydrogel Prodrugs	Three-dimensional network hydrogels.	Key breakage or network expansion.	Local targeting (in situ injection retention) results in a long tumor retention time (several weeks), but the tissue penetration is limited.	It can integrate immune drugs to achieve synergistic treatment.	Long-term biocompatibility needs to be evaluated.
Inorganic Nanoprodrugs	Inorganic nanoparticles such as mesoporous silicon and titanium dioxide.	Modify the orifice gate, and ROS triggers release.	Passive targeting (EPR effect) can enhance targeting through surface modification and has a high drug loading capacity.	It can be integrated with imaging functions, such as MRI contrast and fluorescence labeling.	The long-term safety of inorganic degradation products needs to be verified.

6. Safety Assessment

The safety of ROS-responsive prodrug metabolites is crucial for their clinical translation. Although high concentrations of phenol have potential hepatotoxicity [173], the toxicity of boronate or boronic acid prodrug systems is relatively low. For instance, prodrug **2** can shrink tumors in mice without causing significant damage to the major organs. Sulfonic acid, a metabolite of thione bonds, is highly hydrophilic and is easy to clear [73]. The prodrug **24** constructed based on this method, causes no significant damage to the major organs. In contrast, sulfide metabolites have higher polarity, are excreted more quickly, cause no apparent damage to organs, and have normal serum liver and kidney function indicators. Relatively few studies have been conducted on the safety of diselenide and selenium metabolites. However, the cytotoxicity of organic selenium is significantly lower than that of inorganic selenium [174]. The drug carriers constructed based on this have good biological safety, with no noticeable damage to mouse organs detected in in *vivo* antitumor experiments. Furthermore, many studies cited in this article have achieved therapeutic effects through the augmentation of ROS levels, which seems to contradict the view that "high levels of ROS may promote tumor metastasis". In fact, ROS exert a dual function in the occurrence and progression of tumors; therefore, there is no essential conflict between them and the treatment strategies based on ROS. Specifically, in the initial phases of cancer development, ROS levels that exceed the normal physiological range promote the formation and advancement of tumors [175]. The primary mechanism involves the triggering of epithelial-mesenchymal transition (EMT) in tumor cells by activating signaling pathways like NF-κB and transforming growth factor-β (TGF-β), thereby enhancing the invasion and metastatic abilities of tumor cells [24]. However, when ROS accumulate in large quantities within cells, their biological effects shift to anticancer effects. On the one hand, obstructing signaling pathways linked to proliferation, including the EGF/EGFR and PI3K/Akt pathways [176], impedes cell cycle progression, and such interference involves the arrest of the G2/M phase. It simultaneously reduces the synthesis of nucleotides and ATP, thereby suppressing the proliferative activity of cancer cells. Conversely, activation of the endoplasmic reticulum stress pathway [177], the mitochondrial apoptotic pathway [178], the p53-dependent apoptotic pathway, and the ferroptosis pathway [179,180], induces the demise of cancer cells. The multiple studies presented in this article have demonstrated the abilities of tumor cells to proliferate and migrate after drug treatment. For instance, prodrug **5** had a notable inhibitory impact on the proliferation and migration of MDA-MB-231 and MCF-10A cells and also decreased intracellular ATP content. Overall, the currently constructed ROS-responsive prodrug systems have metabolites with high hydrophilicity, rapid excretion, and low cytotoxicity in normal cells. In animal experiments, they have exhibited low organ toxicity. Moreover, ROS levels induced by treatment do not promote tumor metastasis. This provides strong experimental evidence and theoretical support for the clinical transformation of this type of prodrug system in terms of safety.

7. Conclusion

In conclusion, ROS-responsive DDS enable precise drug release and efficient delivery by exploiting elevated ROS levels in the TME. This presents an innovative approach to developing cancer treatments. This review systematically covers ROS-responsive platforms, from prodrug design and nanocarriers (such as polymers and inorganic nanoparticles) to intelligent hydrogels, highlighting

their core design principles and recent advances. Response units, such as thioketal bonds, diselenide bonds, and phenylboronate esters, facilitate the breaking of chemical bonds or the conversion between hydrophilic and hydrophobic states. Tumor accumulation is enhanced when combined with the EPR effect or targeted modifications. Ultimately, controlled drug release occurs via ROS-triggered cascade reactions. These systems offer significant benefits, including reduced toxicity and side effects compared to traditional chemotherapy, enhanced effectiveness of immunotherapy, and prevention of tumor recurrence. Nonetheless, several key challenges remain: individual differences (tumor heterogeneity and varying ROS levels among patients) necessitate the development of intelligent systems capable of regulating response thresholds and addressing low ROS levels; integrating ROS-enhancing strategies, such as chemodynamic and photodynamic therapy, is essential to improve activation efficiency; adapting to the complex microenvironment requires multiple responsive mechanisms, including pH, enzymes, and GSH, as a single ROS response is insufficient for the dynamic TME; and issues related to the long-term biocompatibility of carrier materials, large-scale manufacturing, and in vivo metabolism warrant further study. Future research should focus on multidisciplinary approaches, employing artificial intelligence to predict personalized drug regimens and biomaterial science to optimize carrier design. The development of integrated diagnostic and therapeutic platforms that incorporate real-time imaging is vital. For clinical translation, establishing standardized evaluation systems is necessary to support the transition from animal experiments to human trials. As nanotechnology, immunology, and precision medicine continue to converge, ROS-responsive delivery systems are poised to overcome current barriers, thereby establishing a new standard for treating tumors and other diseases associated with oxidative stress.

Acknowledgements

Support from the following sources: the project of Haixi Science and Technology Bureau of Qinghai Province (2017-Q4), and the Academic Promotion Program of Shandong First Medical University (nos. 2019LJ003).

Competing Interests

The authors have declared that no competing interest exists.

References

1. Tsai CC, Wang CY, Chang HH, Chang PTS, Chang CH, Chu TY, et al. Diagnostics and therapy for malignant tumors. Biomedicines. 2024; 12: 2659.
2. Kisby T, Borst GR, Coope DJ, Kostarelos K. Targeting the glioblastoma resection margin with locoregional nanotechnologies. Nat Rev Clin Oncol. 2025; 22: 1-21.
3. Zhou Z, Pang Y, Ji J, He J, Liu T, Ouyang L, et al. Harnessing 3D in vitro systems to model immune responses to solid tumours: a step towards improving and creating personalized immunotherapies. Nat Rev Immunol. 2023; 24: 18-32.
4. Kondepudi A, Pekmezci M, Hou X, Scotford K, Jiang C, Rao A, et al. Foundation models for fast, label-free detection of glioma infiltration. Nature. 2024; 637: 439-445.
5. Liu YQ, Wang XL, He DH, Cheng YX. Protection against chemotherapy- and radiotherapy-induced side effects: A review based on the mechanisms and therapeutic opportunities of phytochemicals. Phytomedicine. 2021; 80: 153402.
6. Geynisman DM, Chien C-R, Smieliauskas F, Shen C, Shih Y-CT. Economic evaluation of therapeutic cancer vaccines and immunotherapy: A systematic review. Hum Vaccin Immunother. 2014; 10: 3415-3424.
7. Xu M, Li S. Nano-drug delivery system targeting tumor microenvironment: A prospective strategy for melanoma treatment. Cancer Lett. 2023; 574: 216397.
8. Delahousse J, Skarbek C, Paci A. Prodrugs as drug delivery system in oncology. Cancer Chemother Pharmacol. 2019; 84: 937-958.
9. Guo H, Zhang Z, Chen Y, Yang H, Deng L, Dai J, et al. All-in-one photoacid generators with green/red-light responsiveness and cooperative functionality. Angew Chem Int Ed Engl. 2025; 64: e202425313.
10. Chen Z, Li H, Bian Y, Wang Z, Chen G, Zhang X, et al. Bioorthogonal catalytic patch. Nat Nanotechnol. 2021; 16: 933-941.
11. Ding Z, Guo Z, Zheng Y, Wang Z, Fu Q, Liu Z. Radiotherapy reduces N-oxides for prodrug activation in tumors. J Am Chem Soc. 2022; 144: 9458-9464.
12. Agrawal K, Asthana S, Kumar D. Role of Oxidative Stress in Metabolic Reprogramming of Brain Cancer. Cancers. 2023; 15: 4920.
13. Firouzabadi BM, Gigliobianco MR, Joseph JM, Censi R, Di Martino P. Design of nanoparticles in cancer therapy based on tumor microenvironment properties. Pharmaceutics. 2022; 14: 2708.
14. Zhang Y, Zhou J, Chen X, Li Z, Gu L, Pan D, et al. Modulating tumor-stromal crosstalk via a redox-responsive nanomedicine for combination tumor therapy. J Control Release. 2023; 356: 525-541.
15. Shen TF, Wang YT, Cheng LM, Bode AM, Gao Y, Zhang ST, et al. Oxidative complexity: The role of ROS in the tumor environment and therapeutic implications. Bioorg Med Chem. 2025; 127: 118241.
16. Ma Y, Guo JR, Rao HP, Xin JY, Song XY, Liu R, et al. The 8-oxoguanine DNA glycosylase-synaptotagmin 7 pathway increases extracellular vesicle release and promotes tumour metastasis during oxidative stress. J Extracell Vesicles. 2024; 13: e12505.
17. Wang XH, Fang HQ, Huang ZL, Shang W, Hou TT, Cheng AW, et al. Imaging ROS signaling in cells and animals. J Mol Med. 2013; 91: 917-927.
18. Moloney JN, Cotter TG. ROS signalling in the biology of cancer. Semin Cell Dev Biol. 2018; 80: 50-64.
19. Mittal M, Siddiqui MR, Tran K, Reddy SP, Malik AB. Reactive Oxygen Species in Inflammation and Tissue Injury. Antioxid Redox Signal. 2014; 20: 1126-1167.
20. Zheng Y, Liu H, Lu B, Dong M, Wang X. Targeting reactive oxygen species to ameliorate T cell-mediated inflammation in dry eye syndrome: a novel therapeutic approach. RSC Adv. 2024; 14: 36804-36815.
21. Chávez MD, Tse HM. Targeting mitochondrial-derived reactive oxygen species in T cell-mediated autoimmune diseases. Front Immunol. 2021; 12: 703972.
22. Huang Z, Liu Y, Wang L, Ali A, Yao Q, Jiang X, et al. Supramolecular assemblies mimicking neutrophil extracellular traps for MRSE infection control. Biomaterials. 2020; 253: 120124.
23. Wu C, Xie J, Yao Q, Song Y, Yang G, Zhao J, et al. Intrahippocampal supramolecular assemblies directed bioorthogonal liberation of neurotransmitters to suppress seizures in freely moving mice. Adv Mater. 2024; 36: 2314310.
24. Huang R, Chen H, Liang J, Li Y, Yang J, Luo C, et al. Dual role of reactive oxygen species and their application in cancer therapy. J Cancer. 2021; 12: 5543-5561.
25. Prasad S, Gupta SC, Tyagi AK. Reactive oxygen species (ROS) and cancer: Role of antioxidative nutraceuticals. Cancer Lett. 2017; 387: 95-105.

26. Arfin S, Jha NK, Jha SK, Kesari KK, Ruokolainen J, Roychoudhury S, et al. Oxidative stress in cancer cell metabolism. Antioxidants. 2021; 10: 642.
27. Raimondi V, Ciccarese F, Ciminale V. Oncogenic pathways and the electron transport chain: a dange ROS liaison. Br J Cancer. 2019; 122: 168-181.
28. Corn KC, Windham MA, Rafat M. Lipids in the tumor microenvironment: From cancer progression to treatment. Prog Lipid Res. 2020; 80: 101055.
29. Liao Z, Chua D, Tan NS. Reactive oxygen species: a volatile driver of field cancerization and metastasis. Mol Cancer. 2019; 18: 65.
30. Prabhakar NR, Semenza GL. Adaptive and maladaptive cardiorespiratory responses to continuous and intermittent hypoxia mediated by hypoxia-inducible factors 1 and 2. Physiol Rev. 2012; 92: 967-1003.
31. Yin H, Gu P, Xie Y, You X, Zhang Y, Yao Y, et al. ALKBH5 mediates silica particles-induced pulmonary inflammation through increased m6A modification of Slamf7 and autophagy dysfunction. J Hazard Mater. 2024; 462: 132736.
32. Jere SW, Houreld NN, Abrahamse H. Role of the PI3K/AKT (mTOR and GSK3β) signalling pathway and photobiomodulation in diabetic wound healing. Cytokine Growth Factor Rev. 2019; 50: 52-59.
33. Taniguchi K, Karin M. NF-κB, inflammation, immunity and cancer: coming of age. Nat Rev Immunol. 2018; 18: 309-324.
34. Lin ZY, Xu L, Zhang JF, Li Z, Zhao JS. Novel thioacetal-bridged hollow mesoporous organosilica nanoparticles with ROS-responsive biodegradability for smart drug delivery. Nano. 2019; 14: 1950141.
35. Jiang KX, Wu WH, Xie MR, He H, Sun RY. Fabrication of hyaluronic acid-targeted supramolecular delivery platform with pH and ROS-responsive drug release. Macromol Rapid Commun. 2025; 46: e2500201.
36. Wang H, Gao LF, Fan TJ, Zhang C, Zhang B, Al Hartomy OA, et al. Strategic design of intelligent-responsive nanogel carriers for cancer therapy. ACS Appl Mater Interfaces. 2021; 13: 54621-54647.
37. Tu YL, Xiao X, Dong YS, Li JS, Liu Y, Zong QY, et al. Cinnamaldehyde-based poly(thioacetal): A ROS-awakened self-amplifying degradable polymer for enhanced cancer immunotherapy. Biomaterials. 2022; 289: 121795.
38. Fan Z, Xu H. Recent progress in the biological applications of reactive oxygen species-responsive polymers. Polym Rev. 2019; 60: 114-143.
39. Lv J, Yang Z, Wang CP, Duan JA, Ren LF, Rong GY, et al. Efficient intracellular and in vivo delivery of toxin proteins by a ROS-responsive polymer for cancer therapy. J Control Release. 2023; 355: 160-170.
40. Wei DS, Sun Y, Zhu H, Fu QR. Stimuli-responsive polymer-based nanosystems for cancer theranostics. ACS Nano. 2023; 17: 23223-23261.
41. Pu MJ, Cao H, Zhang HJ, Wang TY, Li YW, Xiao SM, et al. ROS-responsive hydrogels: from design and additive manufacturing to biomedical applications. Mater Horiz. 2024; 11: 3721-3746.
42. Ali I, Rizwan A, Vu TT, Jo SH, Oh CW, Kim YH, et al. NIR-responsive carboxymethyl-cellulose hydrogels containing thioketal-linkages for on-demand drug delivery system. Int. J. Biol. Macromol. 2024; 260: 129549.
43. Yang WT, Yang SH, Jiang LP, Zhou YJ, Yang CL, Deng CJ. Tumor microenvironment triggered biodegradation of inorganic nanoparticles for enhanced tumor theranostics. RSC Adv. 2020; 10: 26742-26751.
44. Wang PF, Gong QJ, Hu JB, Li X, Zhang XJ. Reactive oxygen species (ROS)-responsive prodrugs, probes, and theranostic prodrugs: applications in the ROS-related diseases. J Med Chem. 2021; 64: 298-325.
45. Monteiro SAG, Gois PMP, António JPM. Boronic acids and beyond: ROS-responsive prodrugs as tools for a safer and more effective cancer chemotherapy. Synlett. 2023; 34: 2129-2158.
46. Wei P, Liu LY, Wen Y, Zhao GL, Xue FF, Yuan W, et al. Release of amino-or carboxy-containing compounds triggered by HOCl: application for imaging and drug design. Angew Chem Int Ed Engl. 2019; 58: 4547-4551.
47. Fralish Z, Chen AS, Khan S, Zhou P, Reker D. The landscape of small-molecule prodrugs. Nat Rev Drug Discov. 2024; 23: 365-380.
48. Li SH, Pang J, Sun YJ, Zhang YC, Long YQ. Conditional relay activation of theranostic prodrug by pretargeting bioorthogonal trigger and fluorescence-guided visible light irradiation. Angew Chem Int Ed Engl. 2025; 64: e202422023.
49. Sun Y, Wu Q, Fu Q, Cong H, Shen Y, Yu B, et al. Reactive oxygen species-responsive polyprodrug micelles deliver cell cycle regulators for chemosensitization. Talanta. 2024; 267: 125242.
50. Cao ZY, Li DD, Wang JX, Yang XZ. Reactive oxygen species-sensitive polymeric nanocarriers for synergistic cancer therapy. Acta Biomater. 2021; 130: 17-31.
51. Zu MH, Ma Y, Cannup B, Xie DC, Jung YJ, Zhang JM, et al. Oral delivery of natural active small molecules by polymeric nanoparticles for the treatment of inflammatory bowel diseases. Adv Drug Deliv Rev. 2021; 176: 113887.
52. Zhang P, Liu YX, Feng GB, Li C, Zhou J, Du CY, et al. Controlled interfacial polymer self-assembly coordinates ultrahigh drug loading and zero-order release in particles prepared under continuous flow. Adv Mater. 2023; 35: e2211254.
53. Feng C, Li YJ, Ferdows BE, Patel DN, Ouyang J, Tang ZM, et al. Emerging vaccine nanotechnology: From defense against infection to sniping cancer. Acta Pharm Sin B. 2022; 12: 2206-2223.
54. Gao CX, Wang XJ, Yang B, Yuan W, Huang W, Wu GJ, et al. Synergistic target of intratumoral microbiome and tumor by metronidazole-fluorouridine nanoparticles. ACS Nano. 2023; 17: 7335-7351.
55. Fan ZX, Jin H, Tan XF, Li Y, Shi D, Wang QL, et al. ROS-responsive hierarchical targeting vehicle-free nanodrugs for three-pronged Parkinson's disease therapy. Chem Eng J. 2023; 466: 143245.
56. Ge B, Xie QW, Wu D, Xu JF, Jiao HL, Zhao DW, et al. Hydrogels as drug delivery platforms for orthopedic diseases treatment: A review. Int J Biol Macromol. 2025; 304: 140902.
57. Ganji F, Vasheghani-Farahani E. Hydrogels in controlled drug delivery systems. Iran Polym J. 2009; 18: 63-88.
58. Xu G, Xia H, Chen PY, She W, Zhang HN, Ma J, et al. Thermochromic hydrogels with dynamic solar modulation and regulatable critical response temperature for energy-saving smart windows. Adv Funct Mater. 2022; 32: 21013-21023.
59. Hu C, Zhang FJ, Long LY, Kong QS, Luo RF, Wang YB. Dual-responsive injectable hydrogels encapsulating drug-loaded micelles for on-demand antimicrobial activity and accelerated wound healing. J Control Release. 2020; 324: 204-217.
60. Ding MB, Fan YL, Lv YC, Liu JS, Yu NY, Kong DP, et al. A prodrug hydrogel with tumor microenvironment and near-infrared light dual-responsive action for synergistic cancer immunotherapy. Acta Biomater. 2022; 149: 334-346.
61. Tonga GY, Moyano DF, Kim CS, Rotello VM. Inorganic nanoparticles for therapeutic delivery: Trials, tribulations and promise. Curr Opin Colloid Interface Sci. 2014; 19: 49-55.
62. Lv KX, Hou MM, Kou YF, Yu HY, Liu ML, Zhao TC, et al. Black titania janus mesoporous nanomotor for enhanced tumor penetration and near-infrared light-triggered photodynamic therapy. Acs Nano. 2024; 18: 13910-13923.
63. Song YH, Li YH, Xu Q, Liu Z. Mesoporous silica nanoparticles for stimuli-responsive controlled drug delivery: advances, challenges, and outlook. Int J Nanomedicine. 2017; 12: 87-110.
64. Liu Y, Liu YQ, Zang J, Abdullah AAI, Li YY, Dong HQ. Design strategies and applications of ROS-responsive phenylborate ester-based nanomedicine. ACS Biomater Sci Eng. 2020; 6: 6510-6527.
65. Rinaldi A, Caraffi R, Grazioli MV, Oddone N, Giardino L, Tosi G, et al. Applications of the ROS-responsive thioketal linker for the production of smart nanomedicines. Polymer. 2022; 14: 687.
66. Hu JC, Zhang QH, Mu QQ, Tang YY, Wu Z, Wang GJ. A ROS-sensitive diselenide-crosslinked polymeric nanogel for NIR controlled release. Chin J Polym Sci. 2022; 41: 386-393.
67. Wu YJ, Zhou DF, Qi YX, Xie ZG, Chen XS, Jing XB, et al. Novel multi-sensitive pseudo-poly(amino acid) for effective intracellular drug delivery. RSC Adv. 2015; 5: 31972-31983.
68. Cao S, Christiansen R, Peng X. Substituent effects on oxidation-induced formation of quinone methides from arylboronic ester precursors. Eur J Chem. 2013; 19: 9050-9058.
69. Bio M, Nkepang G, You Y. Click and photo-unclick chemistry of aminoacrylate for visible light-triggered drug release. Chem Commun. 2012; 48: 6517.
70. Chi T, Sang T, Wang Y, Ye Z. Cleavage and noncleavage chemistry in reactive oxygen species (ROS)-responsive materials for smart drug delivery. Bioconjug Chem. 2023; 35: 1-21.
71. Bortoli M, Zaccaria F, Dalla Tiezza M, Bruschi M, Fonseca Guerra C, Bickelhaupt FM, et al. Oxidation of organic diselenides and ditellurides by H_2O_2 for bioinspired catalyst design. Phys Chem Chem Phys. 2018; 20: 20874-20885.
72. Shen S, Yan Z, Wu J, Liu X, Guan G, Zou C, et al. Characterization of ROS metabolic equilibrium reclassifies pan-cancer samples and guides pathway targeting therapy. Front Oncol. 2020; 10: 581197.
73. Liu B, Thayumanavan S. Mechanistic investigation on oxidative degradation of ROS-responsive thioacetal/thioketal moieties and their implications. Cell Rep Phys Sci. 2020; 1: 100271.
74. Tao X, Tang L, Xie M, He H, Xu N, Feng L, et al. Dielectric properties analysis of sulfur-containing models in coal and energy evaluation of their sulfur-containing bond dissociation in microwave field. Fuel. 2016; 181: 1027-1033.

75. Chen JX, Shi Y, Zhang YR, Teng LP, Chen JH. One-pot construction of boronate ester based pH-responsive micelle for combined cancer therapy. Colloids Surf B Biointerfaces. 2016; 143: 285-292.
76. Song CC, Ji R, Du FS, Li ZC. Oxidation-responsive poly(amino ester)s containing arylboronic ester and self-immolative motif: synthesis and degradation study. Macromolecules. 2013; 46: 8416-8425.
77. Shim MS, Xia Y. A Reactive Oxygen Species (ROS)-Responsive Polymer for Safe, Efficient, and Targeted Gene Delivery in Cancer Cells. Angew Chem Int Ed Engl. 2013; 52: 6926-6929.
78. Xiao C, Ding J, Ma L, Yang C, Zhuang X, Chen X. Synthesis of thermal and oxidation dual responsive polymers for reactive oxygen species (ROS)-triggered drug release. Polym Chem. 2015; 6: 738-747.
79. Kim DH, Rozhkova EA, Ulasov IV, Bader SD, Rajh T, Lesniak MS, et al. Biofunctionalized magnetic-vortex microdiscs for targeted cancer-cell destruction. Nat Mater. 2010; 9: 165–171.
80. Ren H, Wu Y, Ma N, Xu H, Zhang X. Side-chain selenium-containing amphiphilic block copolymers: redox-controlled self-assembly and disassembly. Soft Matter. 2012; 8: 1460-1466.
81. Liu J, Pang Y, Zhu Z, Wang D, Li C, Huang W, et al. Therapeutic nanocarriers with hydrogen peroxide-triggered drug release for cancer treatment. Biomacromolecules. 2013; 14: 1627-1636.
82. Cao W, Gu Y, Li T, Xu H. Ultra-sensitive ROS-responsive tellurium-containing polymers. Chem Commun. 2015; 51: 7069-7071.
83. Fang R, Xu H, Cao W, Yang L, Zhang X. Reactive oxygen species (ROS)-responsive tellurium-containing hyperbranched polymer. Polym Chem. 2015; 6: 2817-2821.
84. Wang L, Cao W, Xu HP. Tellurium-containing polymers: towards biomaterials and optoelectronic materials. ChemNanoMat. 2016; 2: 479-488.
85. Lee D, Khaja S, Velasquez Castano JC, Dasari M, Sun C, Petros J, et al. In vivo imaging of hydrogen peroxide with chemiluminescent nanoparticles. Nat Mater. 2007; 6: 765-769.
86. Ciscato LFML, Bartoloni FH, Bastos EL, Baader WJ. Direct kinetic observation of the chemiexcitation step in peroxyoxalate chemiluminescence. J Org Chem. 2009; 74: 8974-8979.
87. Song CC, Ji R, Du FS, Liang DH, Li ZC. Oxidation-accelerated hydrolysis of the ortho ester-containing acid-labile polymers. ACS Macro Lett. 2013; 2: 273-277.
88. Liang KJ, Li XP, Wei DL, Jin CH, Liu CW, Xia CF. Deprotection of benzyl-derived groups via photochemically mesolytic cleavage of C-N and C-O bonds. Chem. 2023; 9: 511-522.
89. Rautio J, Meanwell NA, Di L, Hageman MJ. The expanding role of prodrugs in contemporary drug design and development. Nat Rev Drug Discov. 2018; 17: 559-587.
90. Yao QX, Lin F, Fan XY, Wang YP, Liu Y, Liu ZF, et al. Synergistic enzymatic and bioorthogonal reactions for selective prodrug activation in living systems. Nat Commun. 2018; 9: 5032.
91. Li W, Huang JL, Shen C, Jiang WY, Yang X, Huang JX, et al. Tumor-targeted metabolic inhibitor prodrug labelled with cyanine dyes enhances immunoprevention of lung cancer. Acta Pharm Sin B. 2024; 14: 751-764.
92. Ji XY, Pan ZX, Yu BC, De la Cruz LK, Zheng YQ, Ke BW, et al. Click and release: bioorthogonal approaches to "on-demand" activation of prodrugs. Chem Soc Rev. 2019; 48: 1077-1094.
93. Liu J, Liu MX, Zhang HX, Guo W. High-contrast fluorescence diagnosis of cancer cells/tissues based on β-Lapachone-triggered ROS amplification specific in cancer cells. Angew Chem Int Ed Engl. 2021; 60: 12992-12998.
94. Shi Xe, Zhang X, Zhang X, Guo H, Wang S. The integration of reactive oxygen species generation and prodrug activation for cancer therapy. BIO Integr. 2022; 3: 32–40.
95. Dou K, Lu J, Xing Y, Wang R, Won M, Kim J, et al. Metabolic acidity/H_2O_2 dual-cascade-activatable molecular imaging platform toward metastatic breast tumor malignancy. Angew Chem Int Ed Engl. 2024; 64: e202419191.
96. Xiong WY, Li B, Pan JA, Li DJ, Yuan HH, Wan X, et al. Mitochondrial amount determines doxorubicin-induced cardiotoxicity in cardiomyocytes. Adv Sci. 2025; 12: e2412017.
97. Wu DD, Wang HG, Teng TS, Duan SF, Ji AL, Li YZ. Hydrogen sulfide and autophagy: A double edged sword. Pharmacol Res. 2018; 131: 120-127.
98. Hu QW, Yammani RD, Brown-Harding H, Soto-Pantoja DR, Poole LB, Lukesh J. Mitigation of doxorubicin-induced cardiotoxicity with an H_2O_2-Activated, H_2S-Donating hybrid prodrug. Redox Biol. 2022; 53: 102338.
99. Skarbek C, Serra S, Maslah H, Rascol E, Labruère R. Arylboronate prodrugs of doxorubicin as promising chemotherapy for pancreatic cancer. Bioorg Chem. 2019; 91: 103158.
100. Yao X, Sun W, Yuan Y, Hu J, Fu J, Yin J. Amonafide-based H_2O_2-responsive theranostic prodrugs: Exploring the correlation between H_2O_2 level and anticancer efficacy. Bioorg Chem. 2024; 150: 107560.
101. Liu P, Zhao LW, Kepp O, Kroemer G. Crizotinib-a tyrosine kinase inhibitor that stimulates immunogenic cell death. Oncoimmunology. 2019; 8: 1596652.
102. Bielec B, Poetsch I, Ahmed E, Heffeter P, Keppler BK, Kowol CR. Reactive oxygen species (ROS)-sensitive prodrugs of the tyrosine kinase inhibitor crizotinib. Molecules. 2020; 25: 1149.
103. Zhu JW, Chen JT, Song DM, Zhang WD, Guo JP, Cai GP, et al. Real-time monitoring of etoposide prodrug activated by hydrogen peroxide with improved safety. J Mater Chem B. 2019; 7: 7548-7557.
104. Gong QJ, Li X, Li T, Wu XS, Hu JB, Yang FL, et al. A carbon-carbon bond cleavage-based prodrug activation strategy applied to β-Lapachone for cancer-specific targeting. Angew Chem Int Ed Engl. 2022; 61: e202210001.
105. Xu Z, Wang H, Liu H, Chen H, Jiang B. Synthesis and evaluation of reactive oxygen species sensitive prodrugs of a NAMPT inhibitor FK866. Molecules. 2022; 28: 169.
106. Reshetnikov V, Özkan HG, Daum S, Janko C, Alexiou C, Sauer C, et al. N-alkylaminoferrocene-based prodrugs targeting mitochondria of cancer cells. Molecules. 2020; 25: 2545.
107. Xu HG, Annamadov S, Mokhir A. 4-Ferrocenylaniline-based ROS-responsive prodrugs with anticancer activity. J Organomet Chem. 2022; 964: 122305.
108. Zhang QE, Fan XJ, Qian HM, Xiao SS, Song Q, Wang YC, et al. Synthesis and bio-evaluation of aminoferrocene-based anticancer prodrugs as potent ferroptosis inducers. Inorg Chem Front. 2025; 12: 2368-2386.
109. Qian JQ, Xu ZY, Meng C, Liu Y, Wu HM, Wang YY, et al. Redox-activatable theranostic co-prodrug for precise tumor diagnosis and selective combination chemotherapy. J Med Chem. 2022; 65: 10393-10407.
110. Fu Q, Li H, Duan D, Wang C, Shen S, Ma H, et al. External-radiation-induced local hydroxylation enables remote release of functional molecules in tumors. Angew Chem Int Ed Engl. 2020; 59: 21546-21552.
111. Yang CY, Yu PY, Chen JX, Lu RX, Hai L, Yang ZZ, et al. An oxidation-reduction-triggered thiamine disulfide-based prodrug of 10-hydroxycamptothecin for selective tumor cell locking and therapeutic delivery. Eur J Med Chem. 2025; 284: 117233.
112. Bai HH, Huang WJ, Li JQ, Ji YJ, He SP, Hu HG. Enhancing anticancer treatment: Development of cRGD-Conjugated F-OH-Evo prodrugs for targeted delivery. Bioorg Med Chem. 2024; 107: 117759.
113. Ahmadi M, Potlitz F, Link A, von Woedtke T, Nasri Z, Wende K. Flucytosine-based prodrug activation by cold physical plasma. Arch Pharm. 2022; 355: e2200061.
114. Ahmadi M, Singer D, Potlitz F, Nasri Z, von Woedtke T, Link A, et al. Cold physical plasma-mediated fenretinide prodrug activation confers additive cytotoxicity in epithelial cells. Antioxidants. 2023; 12: 1271.
115. He ZL, Charleton C, Devine RW, Kelada M, Walsh JMD, Conway GE, et al. Enhanced pyrazolopyrimidinones cytotoxicity against glioblastoma cells activated by ROS-generating cold atmospheric plasma. Eur J Med Chem. 2021; 224: 113736.
116. Luo XJ, Chi XQ, Lin YY, Yang ZX, Lin HY, Gao JH. A camptothecin prodrug induces mitochondria-mediated apoptosis in cancer cells with cascade activations. Chem Commun. 2021; 57: 11033-11036.
117. Thapa P, Li MJ, Bio M, Rajaputra P, Nkepang G, Sun YJ, et al. Far-red light-activatable prodrug of paclitaxel for the combined effects of photodynamic therapy and site-specific paclitaxel chemotherapy. J Med Chem. 2016; 59: 3204-3214.
118. Yoon MS, Lee YJ, Shin HJ, Park CW, Han SB, Jung JK, et al. Recent advances and challenges in controlling the spatiotemporal release of combinatorial anticancer drugs from nanoparticles. Pharmaceutics. 2020; 12: 1156.
119. Dabkeviciute G, Petrikaite V. Insights into 2D and 3D cell culture models for nanoparticle-based drug delivery to glioblastoma. Biochem Pharmacol. 2025; 237: 116931.
120. Geven M, D'Arcy R, Turhan ZY, El-Mohtadi F, Alshamsan A, Tirelli N. Sulfur-based oxidation-responsive polymers. Chemistry, (chemically selective) responsiveness and biomedical applications. Eur Polym J. 2021; 149: 110387.
121. Gong YH, Shu M, Xie JH, Zhang C, Cao Z, Jiang ZZ, et al. Enzymatic synthesis of PEG-poly(amine--thioether esters) as highly efficient pH and ROS dual-responsive nanocarriers for anticancer drug delivery. J Mater Chem B. 2019; 7: 651-664.
122. Wang JH, Li DD, Tao W, Lu Y, Yang XZ, Wang J. Synthesis of an oxidation-sensitive polyphosphoester bearing thioether group for triggered drug release. Biomacromolecules. 2019; 20: 1740-1747.

123. Dai G, Chu JCH, Chan CKW, Choi CHJ, Ng DKP. Reactive oxygen species-responsive polydopamine nanoparticles for targeted and synergistic chemo and photodynamic anticancer therapy. Nanoscale. 2021; 13: 15899-15915.
124. Yu L, Ke HL, Du FS, Li ZC. Redox-responsive fluorescent polycarbonates based on selenide for chemotherapy of triple-negative breast cancer. Biomacromolecules. 2019; 20: 2809-2820.
125. Hu T, Liu LW, Zhang C, Feng QY, Wang QY, Zhang JL, et al. Self-assembled α-tocopherol succinate dimer nanoparticles combining doxorubicin for increasing chemotherapy/oxidative therapy in 3D tumor spheroids. J Drug Deliv Sci Technol. 2023; 84: 104454.
126. Pan QQ, Deng X, Gao WX, Chang J, Pu YJ, He B. ROS triggered cleavage of thioketal moiety to dissociate prodrug nanoparticles for chemotherapy. Colloids Surf B Biointerfaces. 2020; 194: 111223.
127. Mei H, Cai SS, Huang DN, Gao HL, Cao J, He B. Carrier-free nanodrugs with efficient drug delivery and release for cancer therapy: From intrinsic physicochemical properties to external modification. Bioact Mater. 2022; 8: 220-240.
128. Dou L, Liu H, Wang K, Liu J, Liu L, Ye J, et al. Albumin binding revitalizes NQO1 bioactivatable drugs as novel therapeutics for pancreatic cancer. J Control Release. 2022; 349: 876-889.
129. Yin W, Ke WD, Chen WJ, Xi LC, Zhou QH, Mukerabigwi JF, et al. Integrated block copolymer prodrug nanoparticles for combination of tumor oxidative stress amplification and ROS-responsive drug release. Biomaterials. 2019; 195: 63-74.
130. Wang B, Chen K, Zhang QF, Gu L, Luo Q, Li ZQ, et al. ROS-responsive amphiphilic block copolymer-drug conjugate: Design, synthesis and potential as an efficient drug delivery system via a positive feedback strategy. Chem Eng J. 2021; 425: 131453.
131. Li J, Zong QY, Zhao ZY, Yuan YY. A dual-amplified ROS-responsive nanosystem with self-accelerating drug release for synergistic chemotherapy. Chem Commun. 2023; 59: 3142-3145.
132. Kim Y, Uthaman S, Pillarisetti S, Noh K, Huh KM, Park IK. Bioactivatable reactive oxygen species-sensitive nanoparticulate system for chemo-photodynamic therapy. Acta Biomater. 2020; 108: 273-284.
133. Pei P, Sun CY, Tao W, Li J, Yang XZ, Wang J. ROS-sensitive thioketal-linked polyphosphoester-doxorubicin conjugate for precise phototriggered locoregional chemotherapy. Biomaterials. 2019; 188: 74-82.
134. Huang LL, Wan JQ, Wu HH, Chen XN, Bian Q, Shi LL, et al. Quantitative self-assembly of photoactivatable small molecular prodrug cocktails for safe and potent cancer chemo-photodynamic therapy. Nano Today. 2021; 36: 101030.
135. Diao SC, Liu YX, Guo ZX, Xu ZW, Shen JL, Zhou W, et al. Prolonging treatment window of photodynamic therapy with self-amplified H_2O_2-activated photodynamic/chemo combination therapeutic nanomedicines. Adv Healthc Mater. 2023; 12.
136. He Y, Wang J, Wang S, Yu K, Zhou J, Wang J, et al. Natural mussel protein-derived antitumor nanomedicine with tumor-targeted bioadhesion and penetration. Nano Today. 2023; 48: 101700.
137. Li Y, Lin L, Xie J, Wei L, Xiong S, Yu K, et al. ROS-triggered self-assembled nanoparticles based on a chemo-sonodynamic combinational therapy strategy for the noninvasive elimination of hypoxic tumors. ACS Appl Mater Interfaces. 2023; 15: 15893-15906.
138. Zhang ZT, Wang RY, Huang XX, Luo RJ, Xue JW, Gao J, et al. Self-delivered and self-monitored chemo-photodynamic nanoparticles with light-triggered synergistic antitumor therapies by downregulation of HIF-1α and depletion of GSH. ACS Appl Mater Interfaces. 2020; 12: 5680-5694.
139. Yu J, Xiao H, Yang Z, Qiao C, Zhou B, Jia Q, et al. A potent strategy of combinational blow toward enhanced cancer chemo-photodynamic therapy via sustainable GSH elimination. Small. 2021; 18: e2106100.
140. Wahnou H, El Kebbaj R, Liagre B, Sol V, Limami Y, Duval RE. Curcumin-based nanoparticles: advancements and challenges in tumor therapy. Pharmaceutics. 2025; 17: 114.
141. He QY, Chen J, Yan JH, Cai SD, Xiong HJ, Liu YF, et al. Tumor microenvironment responsive drug delivery systems. Asian J Pharm Sci. 2020; 15: 416-448.
142. Chen M, Wang C, Wang X, Tu Z, Ding Z, Liu Z. An "and" logic-gated prodrug micelle locally stimulates antitumor immunity. Adv Mater. 2023; 36: e2307818.
143. Zhang N, Wang D, Jing X, Yang T, Yang H, Meng L. pH/ROS dual-responsive polymer–drug-based nanocarriers: Click-reaction preparation and fluorescence imaging-guided chemotherapy and photodynamic therapy. ACS Appl Bio Mater. 2021; 4: 6294-6303.
144. Tan JB, Jing P, Xiao X, Liao YL, Liao CY, Zhang SY. Cross-linked lipoic acid nanocapsules serve as H_2O_2 amplifier to strengthen the H_2O_2-sensitive prodrug activation. Sci China Chem. 2023; 66: 2654-2663.
145. Jiao BB, Liu KP, Gong HT, Ding ZS, Xu X, Ren J, et al. Bladder cancer selective chemotherapy with potent NQO1 substrate co-loaded prodrug nanoparticles. J Control Release. 2022; 347: 632-648.
146. Wang J, Zhang HX, Lv JZ, Zheng Y, Li MY, Yang G, et al. A tumor-specific ROS self-supply enhanced cascade-responsive prodrug activation nanosystem for amplified chemotherapy against multidrug-resistant tumors. Acta Biomater. 2023; 164: 522-537.
147. Xu XY, Zeng ZS, Ding X, Shan T, Liu QX, Chen MX, et al. Reactive oxygen species-activatable self-amplifying Watson-Crick base pairing-inspired supramolecular nanoprodrug for tumor-specific therapy. Biomaterials. 2021; 277: 121128.
148. Lu NN, Xi LC, Zha ZS, Wang YH, Han XH, Ge ZS. Acid-responsive endosomolytic polymeric nanoparticles with amplification of intracellular oxidative stress for prodrug delivery and activation. Biomater Sci. 2021; 9: 4613-4629.
149. Luan TT, Cheng LL, Cheng J, Zhang XY, Cao YF, Zhang XD, et al. Tailored design of an ROS-responsive drug release platform for enhanced tumor therapy via "sequential induced activation processes". ACS Appl Mater Interfaces. 2019; 11: 25654-25663.
150. Hu YR, Zhao XM, Liu P. Design of diselenide-containing polyprodrug and its pH/redox co-triggered degradation and slow drug release for tumor-specific chemotherapy. Colloids Surf A Physicochem Eng Asp. 2024; 695: 134308.
151. Yang YC, Tian Q, Wu SQ, Li YX, Yang K, Yan Y, et al. Blue light-triggered Fe^{2+}-release from monodispersed ferrihydrite nanoparticles for cancer iron therapy. Biomaterials. 2021; 271: 120739.
152. Walling SA, Um W, Corkhill CL, Hyatt NC. Fenton and Fenton-like wet oxidation for degradation and destruction of organic radioactive wastes. Npj Mater Degrad. 2021; 5: 50.
153. Ramalho MJ, Bravo M, Loureiro JA, Lima J, Pereira MC. Transferrin-modified nanoparticles for targeted delivery of Asiatic acid to glioblastoma cells. Life Sci. 2022; 296: 120435.
154. Zhang XM, Fang Y, Rong DD, Li J, Li Z, Qiu HD, et al. A novel taxane SB-T-101141 triggers a noncanonical ferroptosis to overcome paclitaxel resistance of breast cancer via iron homeostasis-related KHSRP. Cell Death Dis. 2025; 16: 403.
155. Zhang BB, Liu H, Wang YF, Zhang Y. ROS-responsive and self-catalytic nanocarriers for a combination of chemotherapy and reinforced ferroptosis against breast cancer. ACS Biomater Sci Eng. 2024; 10: 6352-6362.
156. Zheng YF, Qin C, Li F, Qi JX, Chu XY, Li H, et al. Self-assembled thioether-bridged paclitaxel-dihydroartemisinin prodrug for amplified antitumor efficacy-based cancer ferroptotic-chemotherapy. Biomater Sci. 2023; 11: 3321-3334.
157. Qin Y, Liu N, Wang FH, Gao ZP, Luo C, Tian CT, et al. Self-amplifying ROS-responsive SN38 prodrug nanoparticles for combined chemotherapy and ferroptosis in cancer treatment. Carbon. 2025; 235: 120099.
158. Jiang Y, Krishnan N, Heo J, Fang RH, Zhang LF. Nanoparticle-hydrogel superstructures for biomedical applications. J Control Release. 2020; 324: 505-521.
159. Xie S, Wei L, Liu Y, Meng J, Cao W, Qiu B, et al. Size-tunable nanogels for cascaded release of metronidazole and chemotherapeutic agents to combat Fusobacterium nucleatum-infected colorectal cancer. J Control Release. 2024; 365: 16-28.
160. Wang S, Liu Y, Sun Q, Zeng B, Liu C, Gong L, et al. Triple cross-linked dynamic responsive hydrogel loaded with selenium nanoparticles for modulating the inflammatory microenvironment via PI3K/Akt/NF-κB and MAPK signaling pathways. Adv Sci. 2023; 10: e2303167.
161. Regato-Herbella M, Morhenn I, Mantione D, Pascuzzi G, Gallastegui A, Valle ABCD, et al. ROS-responsive 4D printable acrylic thioether-based hydrogels for smart drug release. Chem Mater. 2023; 36: 1262-1272.
162. Rothe R, Xu Y, Wodtke J, Brandt F, Meister S, Laube M, et al. Programmable release of chemotherapeutics from ferrocene-based injectable hydrogels slows melanoma growth. Adv Healthc Mater. 2024; 13: e2400265.
163. Li F, Ding J, Li Z, Rong Y, He C, Chen X. ROS-responsive thermosensitive polypeptide hydrogels for localized drug delivery and improved tumor chemoimmunotherapy. Biomater Sci. 2024; 12: 3100-3111.
164. Ali I, Rizwan A, Vu TT, Jo SH, Oh CW, Kim YH, et al. NIR-responsive carboxymethyl-cellulose hydrogels containing thioketal-linkages for on-demand drug delivery system. Int J Biol Macromol. 2024; 260: 129549.
165. Zhao Y, Yao Q, Chen J, Zhang R, Song J, Gao Y. Intracellular fluorogenic supramolecular assemblies for self-reporting bioorthogonal prodrug activation. Biomater Sci. 2022; 10: 5662-5668.
166. Unnikrishnan G, Joy A, Megha M, Kolanthai E, Senthilkumar M. Exploration of inorganic nanoparticles for revolutionary drug delivery applications: a critical review. Discov Nano. 2023; 18: 157.

167. Spiridon IA, Caruntu ID, Spiridon I, Braescu R. Insight into potential biomedical application of mesoporous materials. Pharmaceutics. 2022; 14: 2382.
168. Wang Y, Zhao QF, Han N, Bai L, Li J, Liu J, et al. Mesoporous silica nanoparticles in drug delivery and biomedical applications. Int J Biol Macromol. 2015; 11: 313-327.
169. Zhang RY, Elzatahry AA, Al-Deyab SS, Zhao DY. Mesoporous titania: From synthesis to application. Nano Today. 2012; 7: 344-366.
170. Huang Y, Nahar S, Alam MDM, Hu S, McVicar DW, Yang D. Reactive oxygen species-sensitive biodegradable mesoporous silica nanoparticles harboring TheraVac elicit tumor-specific immunity for colon tumor treatment. Acs Nano. 2023; 17: 19740-19752.
171. Shi JJ, Chen ZY, Wang BH, Wang L, Lu TT, Zhang ZZ. Reactive oxygen species-manipulated drug release from a smart envelope-type mesoporous titanium nanovehicle for tumor sonodynamic-chemotherapy. ACS Appl Mater Interfaces. 2015; 7: 28554-28565.
172. Hu JJ, Lei Q, Peng MY, Zheng DW, Chen YX, Zhang XZ. A positive feedback strategy for enhanced chemotherapy based on ROS-triggered self-accelerating drug release nanosystem. Biomaterials. 2017; 128: 136-146.
173. Moridani MY, Siraki A, O'Brien PJ. Quantitative structure toxicity relationships for phenols in isolated rat hepatocytes. Chem Biol Interact. 2003; 145: 213-223.
174. Hadrup N, Ravn-Haren G. Toxicity of repeated oral intake of organic selenium, inorganic selenium, and selenium nanoparticles: A review. J Trace Elem Med Biol. 2023; 79: 127235.
175. Miao N, Kang Z, Wang Z, Yu W, Liu T, Kong L, et al. Mitochondrial reactive oxygen species promote cancer metastasis and tumor microenvironment immunosuppression through gasdermin D. Cell Death Discov. 2025; 11: 219.
176. Lee YJ, Jeong HY, Kim YB, Lee YJ, Won SY, Shim JH, et al. Reactive oxygen species and PI3K/Akt signaling play key roles in the induction of Nrf2-driven heme oxygenase-1 expression in sulforaphane-treated human mesothelioma MSTO-211H cells. Food Cosmet Toxicol. 2012; 50: 116-123.
177. Ding W, Yang L, Zhang MM, Gu Y. Reactive oxygen species-mediated endoplasmic reticulum stress contributes to aldosterone-induced apoptosis in tubular epithelial cells. Biochem Biophys Res Commun. 2012; 418: 451-456.
178. Wang JP, Hsieh CH, Liu CY, Lin KH, Wu PT, Chen KM, et al. Reactive oxygen species-driven mitochondrial injury induces apoptosis by teroxirone in human non-small cell lung cancer cells. Oncol Lett. 2017; 14: 3503-3509.
179. Johnson TM, Yu ZX, Ferrans VJ, Finkel T. Reactive oxygen species are downstream mediators of p53-dependent apoptosis. Proc Natl Acad Sci U S A. 1996; 21: 11848-11852.
180. Wang Z, Ren X, Li Y, Qiu L, Wang D, Liu A, et al. Reactive oxygen species amplifier for apoptosis-ferroptosis mediated high-efficiency radiosensitization of tumors. ACS Nano. 2024; 18: 10288-10301.